Development/Plasticity/Repair

Macrophages Promote Repair of Inner Hair Cell Ribbon Synapses following Noise-Induced Cochlear Synaptopathy

Vijayprakash Manickam,[1] Dinesh Y. Gawande,[1] Andrew R. Stothert,[1] Anna C. Clayman,[2] Lyudmila Batalkina,[1] Mark E. Warchol,[2] Kevin K. Ohlemiller,[2] and Tejbeer Kaur[1]

[1]Department of Biomedical Sciences, School of Medicine, Creighton University, Omaha, Nebraska 68178, and [2]Department of Otolaryngology, School of Medicine, Washington University, St. Louis, Missouri 63110

Resident cochlear macrophages rapidly migrate into the inner hair cell synaptic region and directly contact the damaged synaptic connections after noise-induced synaptopathy. Eventually, such damaged synapses are spontaneously repaired, but the precise role of macrophages in synaptic degeneration and repair remains unknown. To address this, cochlear macrophages were eliminated using colony stimulating factor 1 receptor (CSF1R) inhibitor, PLX5622. Sustained treatment with PLX5622 in $CX_3CR1^{GFP/+}$ mice of both sexes led to robust elimination of resident macrophages (~94%) without significant adverse effects on peripheral leukocytes, cochlear function, and structure. At 1 day (d) post noise exposure of 93 or 90 dB SPL for 2 hours, the degree of hearing loss and synapse loss were comparable in the presence and absence of macrophages. At 30 d after exposure, damaged synapses appeared repaired in the presence of macrophages. However, in the absence of macrophages, such synaptic repair was significantly reduced. Remarkably, on cessation of PLX5622 treatment, macrophages repopulated the cochlea, leading to enhanced synaptic repair. Elevated auditory brainstem response thresholds and reduced auditory brainstem response Peak 1 amplitudes showed limited recovery in the absence of macrophages but recovered similarly with resident and repopulated macrophages. Cochlear neuron loss was augmented in the absence of macrophages but showed preservation with resident and repopulated macrophages after noise exposure. While the central auditory effects of PLX5622 treatment and microglia depletion remain to be investigated, these data demonstrate that macrophages do not affect synaptic degeneration but are necessary and sufficient to restore cochlear synapses and function after noise-induced synaptopathy.

Key words: **cochlea; inner hair cells; macrophages; noise-induced hearing loss; PLX5622; ribbon synapses**

Significance Statement

The synaptic connections between cochlear inner hair cells and spiral ganglion neurons can be lost because of noise over exposure or biological aging. This loss may represent the most common causes of sensorineural hearing loss also known as hidden hearing loss. Synaptic loss results in degradation of auditory information, leading to difficulty in listening in noisy environments and other auditory perceptual disorders. We demonstrate that resident macrophages of the cochlea are necessary and sufficient to restore synapses and function following synaptopathic noise exposure. Our work reveals a novel role for innate-immune cells, such as macrophages in synaptic repair, that could be harnessed to regenerate lost ribbon synapses in noise- or age-linked cochlear synaptopathy, hidden hearing loss, and associated perceptual anomalies.

Received June 26, 2022; revised Feb. 7, 2023; accepted Feb. 10, 2023.

Author contributions: V.M., D.Y.G., A.R.S., and T.K. designed research; V.M., D.Y.G., A.R.S., A.C.C., L.B., and T.K. performed research; V.M., D.Y.G., A.R.S., A.C.C., and T.K. analyzed data; V.M., M.E.W., K.K.O., and T.K. wrote the first draft of the paper; V.M., M.E.W., K.K.O., and T.K. edited the paper.

This work was supported by National Institute on Deafness and Other Communication Disorders Grants R03 DC015320 and R01 DC019918, Nebraska State Funds, and Bellucci Translational Hearing Research Funds to T.K. This work was also supported by the Translational Hearing Center at Creighton University, Boys Town National Research Hospital, and University of Nebraska Medical Center with CoBRE Award GM139762 from the National Institute of General Medical Science, a component of the National Institutes of Health. This investigation is solely the responsibility of the authors and does not necessarily represent the official views of any supporting institution. We thank Sharon Kujawa (Massachusetts Eye and Ear) and the Translational Hearing Research Group, Creighton University, Omaha, Nebraska for constructive criticism that tremendously improved the manuscript.

The authors declare no competing financial interests.

Correspondence should be addressed to Tejbeer Kaur at TejbeerKaur@creighton.edu.

https://doi.org/10.1523/JNEUROSCI.1273-22.2023

Introduction

Sensorineural hearing loss reflects damage to the sensory receptors (i.e., hair cells and/or spiral ganglion neurons [SGNs]) or to the ribbon synapses between inner hair cells (IHCs) and SGNs. Noise trauma is the most common preventable cause of hearing loss. It has been suggested that at least 10 million adults (6%) in the United States under age 70, and perhaps as many as 40 million adults (24%), have features of hearing loss from exposure to loud noise; and 12% or more of the world population is at risk for noise-induced loss of hearing (Le et al., 2017; Sliwinska-Kowalska and Zaborowski, 2017; GBD 2019 Hearing Loss Collaborators, 2021; World Health Organization, 2021). Research in rodents and primate models and in humans has shown that IHC ribbon synapses are vulnerable to rapid and

primary degeneration after exposure to moderate noise (Kujawa and Liberman, 2009; Lin et al., 2011; Liberman et al., 2015; Shi et al., 2015; Viana et al., 2015; Bramhall et al., 2017; Valero et al., 2017; Wu et al., 2021). Noise-induced synaptic damage can precede hair cell loss or threshold elevation (Kujawa and Liberman, 2009) and can lead to the selective degeneration of high threshold afferent nerve fibers with low spontaneous rates in guinea pigs (Furman et al., 2013) but not in mice (Suthakar and Liberman, 2021) and progressive loss of SGN cell bodies over a period of months to years (Kujawa and Liberman, 2009). This type of cochlear synaptopathy is known as noise-induced hidden hearing loss because it is not readily diagnosed by the threshold audiograms, the standard clinical examination for hearing loss. This condition can be detected histologically by counting juxtaposed presynaptic and postsynaptic markers in fixed cochleae. Alternatively, persistent reduction of auditory brainstem response (ABR) Peak I amplitude even after complete recovery of ABR thresholds has been taken to represent a proxy functional assay (Kujawa and Liberman, 2009; Sergeyenko et al., 2013; Fernandez et al., 2020). The consequences of hidden hearing loss include difficulty listening in noisy environments and may be key to the generation of tinnitus, hyperacusis, and other associated perceptual anomalies (Hickox and Liberman, 2014; Bramhall et al., 2018, 2019, 2020). Some degree of natural synaptic repair can occur following noise exposure, which may be related to noise level, duration, age, and sex at exposure, levels of neurotrophic molecules or differences in species and strain of the animal model (Shi et al., 2013, 2015; Song et al., 2016; Kaur et al., 2019; Kim et al., 2019; Hickman et al., 2020, 2021). Nonetheless, the precise mechanisms that regulate spontaneous synapse repair remain poorly understood.

We have demonstrated that macrophages migrate into the damaged IHC-synaptic region immediately after synaptopathic noise exposure, and directly contact the damaged synaptic connections. The spontaneous repair of these synapses is dependent on fractalkine signaling (Kaur et al., 2019), but the functional consequences of macrophage contacts with those damaged synapses remain unclear. In the present study, we aimed to confirm the functions of macrophages in preventing or worsening loss of ribbon synapses and in the repair of damaged ribbon synapses after noise-induced hearing loss. To this aim, we used chronic pharmacological selective inhibition of the colony-stimulating factor 1 receptor (CSF1R), which is essential for macrophage survival (Stanley et al., 1997; Elmore et al., 2014; Rojo et al., 2019) by systemic PLX5622 treatment and withdrawal of CSF1R inhibitor for macrophage elimination and repopulation, respectively (Valdearcos et al., 2014; Dagher et al., 2015; Elmore et al., 2015). Our data suggest that macrophage depletion does not affect synaptic loss, but that macrophages are both necessary and sufficient for restoring hearing and synapses following noise-induced cochlear synaptopathy. These findings represent novel and clinically feasible approach of macrophage-based immunotherapy to restore synapses and function in hidden hearing loss.

Materials and Methods

Mice

Studies used in-house bred $CX_3CR1^{GFP/+}$ heterozygous mice on a C57BL/6J background (The Jackson Laboratory, stock #005582). These mice express Enhance Green Fluorescent Protein (EGFP) in cochlear resident macrophages, monocytes, microglia, dendritic cells, and NK cells under the control of endogenous *Cx3cr1* locus. Expression of CSF1R in the adult cochlea was examined using *CSF1R-EGFP* mice (The Jackson Laboratory, stock #018549). Efforts were made to minimize animal suffering and to reduce the numbers of animals used. Animals were housed under a 12 h light/12 h dark cycle and fed *ad libitum*, unless specified. All aspects of animal care, procedure, and treatment were conducted according to guidelines of the Animal Studies Committee of Creighton University. $CX_3CR1^{GFP/+}$ heterozygous mice were identified by genotyping as described previously (Kaur et al., 2015).

Study design and PLX5622-induced depletion of cochlear macrophages and repopulation of macrophages in the cochlea following cessation of PLX5622 treatment

$CX_3CR1^{GFP/+}$ heterozygous mice of both sexes at 5-6 weeks of age were used for experiments. Following assessment of baseline hearing thresholds, mice were fed on either standard nutritionally complete rodent diet (AIN-76A formulation, referred to as control chow) or on AIN-76A chow that contained 1.2 g/kg of PLX5622 (hemifumarate salt of 98% purity, or no salt of 99.39% purity, catalog #HY-114153A, MedChemExpress, referred to as PLX5622 chow). PLX5622 is a selective antagonist of CSF1R, that regulates macrophage development, survival, and maintenance (Elmore et al., 2014). Both control and PLX5622 chows were formulated, irradiated, and supplied by Research Diets. Following 2 weeks on chow, which led to a robust elimination of cochlear resident macrophages, both control and PLX5622 fed mice were exposed to noise and the special chows were maintained until the end of the experiment for sustained macrophage depletion. In a cohort of PLX5622-fed mice, PLX5622 chow was replaced with control chow (referred as PLX5622 to control chow) immediately after noise exposure to allow repopulation of macrophages in the cochlea lacking macrophages. The study design generated three noise-exposed experimental groups: control (macrophages present), PLX5622 (macrophages absent), and PLX5622 to control (macrophages repopulated). Additionally, sham-exposed age-matched mice per experimental group served as controls. Body weight and hearing were assessed at baseline, and 1, 15, or 30 days post noise exposure (DPNE). Mice were killed and temporal bones were isolated at 1, 15, or 30 DPNE for cochlear microdissections or cryosectioning and histology to examine hair cells, synapses, macrophages, and SGNs.

Electrophysiological recordings

Auditory brainstem responses (ABRs) and distortion product otoacoustic emissions (DPOAEs) were measured by an observer who was "blinded" to the experimental conditions of each animal. Mice were anesthetized with an intraperitoneal injection of ketamine/xylazine (Patterson Veterinary) cocktail (100 and 20 mg/kg, respectively; dose: 0.1 ml/20 g body weight), following procedures described in our previous publications (Kaur et al., 2019). ABR thresholds and DPOAE levels were measured before noise exposure, at 1 DPNE (to verify degree of hearing loss), and at 2 or 4 weeks after noise exposure, to quantify recovery of hearing.

ABRs. Anesthetized mice were placed on a heating pad set at 37°C, and eyes were lubricated with an ophthalmic ointment (Artificial Tears) to avoid drying because of anesthesia. Subcutaneous needle electrodes were placed behind the right pinna (reference) and vertex (active). A ground electrode was placed near the tail of the mouse. A TDT Multi Field (MF1) speaker was set at 10 cm from the right pinna and calibrated with PCB quarter-inch free field calibration microphone before recordings. Stimuli of 5 ms tone pips (0.5 ms $\cos^2$ rise-fall) were delivered at 21/s with alternating stimulus polarity using an RZ6-A-P1 Bioacoustic system and Medusa4Z pre-amplifier (Tucker-Davis Technologies). Recorded electrical responses at a sampling rate of 12 kilohertz (kHz) were filtered (300 Hz to 3 kHz) and averaged using BioSigRZ software (Tucker-Davis Technologies). The sound level was decreased in 5 dB steps from 100 decible sound pressure level (dB SPL) down to 10 decible SPL. At each sound level, 512-1024 responses were averaged, and response waveforms are discarded as artifacts if the Peak to-peak voltage exceeded 15 μV. Thresholds at 5.6, 8.0, 11.2, 16.0, 22.6, and 32.0 kHz were determined by a single observer who noted the lowest sound level at which a recognizable Peak 1 (P1) waveform could be obtained. Waveforms were confirmed as auditory-evoked responses by their increasing latency and decreasing amplitude as the intensity of the stimulus is lowered. ABR

thresholds refer to the lowest SPL that can generate identifiable electrical response waves. These threshold values (actual or assigned) were used to calculate the mean ABR thresholds at each stimulus frequency. Threshold shifts were calculated by subtracting baseline thresholds from thresholds at 1, 15, and 30 DPNE at all the stimulus frequencies.

Input/output (I/O) neural response. Methods followed those described by Kaur et al. (2019). Briefly, ABR Peak 1 component was identified, and the peak to trough amplitudes and latencies were computed by offline analysis of stored ABR waveforms. ABR Peak I amplitude and latency versus-stimulus level (ABR I/O) data were computed at 16 and 22.6 kHz for sound levels ranging from 100 dB SPL up to the hearing thresholds, unless otherwise specified. Suprathreshold ABR Peak 1 amplitude and latency were analyzed at 93 or 90 dB SPL stimulus level and plotted as a function of postexposure recovery times.

DPOAEs. Anesthetized mice were placed on a heating pad set at 37°C, and eyes were lubricated with an ophthalmic ointment (Artificial Tears) to avoid drying because of anesthesia. Stimuli were presented at 5-40 kHz and delivered to the right ear by a custom coupling insert RZ6-A-P1 bioacoustic system (Tucker-Davis Technologies). Electrostatic loudspeakers (EC1) were calibrated with ER10B+ Etymotic low noise probe and microphone before recordings. Distortion product grams (2f1-f2) were obtained for f2 ranging from 5 to 40 kHz, with a frequency ratio of f2/f1 of 1.2 and L1-L2 = 10 dB. Recordings were performed using BioSigRZ software (Tucker-Davis Technologies). Following ABR/DPOAE recordings, animals were placed on a heating pad at 37°C and monitored until they regained activity and then returned to animal research facility.

Noise exposure

Awake, unrestrained mice were exposed for 2 h to an octave band-noise (8-16 kHz) at graded noise levels (90 or 93 dB SPL). Noise exposures were performed in a foam-lined, single-walled soundproof room (WhisperRoom). Briefly, mice were placed singly or in pairs in modified subdivided cages (food, water, bedding removed) positioned up to two cages at once directly under an exponential horn (JBL). Noise was generated digitally using custom Labview routines and a Lynx E22 sound card (running on a PC), filtered pure tone (8-16 kHz), and amplified (D-150A power amplifier, Crown Audio) that drive the speaker through an exponential horn (JBL). Before each exposure, the noise was calibrated to target SPL using a quarter-inch condenser microphone (PCB). SPLs varied by ±1 dB across the subdivisions in the cage. Unexposed mice served as age-matched sham controls.

Tissue harvesting and processing

Mice were deeply anesthetized with lethal doses of pentobarbital sodium (Trade Name-Fatal Plus, Patterson Veterinary). Before respiratory arrest, mice were perfused by transcardiac route with PBS (Fisher Scientific, catalog #BP661-10) or 4% PFA (Fisher Scientific, catalog #50980495) in 0.1 M PB solution. Temporal bones, spleen, blood, and bone for bone marrow were harvested. Blood was collected via terminal cardiac puncture before perfusion. Withdrawn blood was immediately incubated for 15 min at room temperature in a 0.2% Heparin solution (Scien Cell, catalog #0863) to prevent coagulation. Heparinized blood was treated with 1× Red Blood Cell Lysis Buffer (Invitrogen, catalog #00-4333-57) for 5 min at room temperature with gentle agitation and subsequently thoroughly washed with PBS, pelleted at 300 × *g* for 5 min, and then resuspended in 1 ml of cell staining buffer (BioLegend, catalog #420201) before cell counting, immunostaining, and flow cytometry. Bone marrow was removed from the femur and tibia into PBS and dissociated by gentle pipetting. For splenocytes, the spleen was crushed in PBS using a syringe plunger. Cell suspensions were filtered through a 70 µm cell strainer; RBCs were lysed by incubating with RBC lysis buffer for 10 min at room temperature. The cells were collected after centrifuging at 800 × *g* for 10 min at 4°C.

For fluorescent immunolabeling of cochlear synapses, excised temporal bones were postfixed in 4% PFA for 15-20 min on ice and decalcified in 0.1 M EDTA (Fisher Scientific, catalog #AC327205-000) overnight for ~16 h. For macrophage and SGN immunolabeling in cochlear frozen mid-modiolar sections, temporal bones were fixed for 3-4 h at room temperature and decalcified for 3-5 d. The temporal bones were rinsed 3 times with PBS and appropriate fluorescent immunohistochemistry was performed.

Flow cytometry

Single-cell suspensions of lysed blood, bone marrow, and spleen were incubated for 10 min on ice in a blocking solution containing 2% Fc Block (BD Biosciences, catalog #553142) and subsequently stained with a combination of fluorophore-conjugated primary antibodies against CD45 (BD Biosciences, catalog #559864, 1:5), CD11b (BioLegend, catalog #101241, 1:5), CD3 (BD Biosciences, catalog #562332, 1:20), CD19 (BioLegend, catalog #115539, 1:5), and Live/Dead Fixable Violet Dead Cell Stain (Invitrogen, L34963, 1:2000). Samples were incubated in the dark and on ice for 30 min. After completion of staining, cells were washed with 1 ml of cell staining buffer (BioLegend, catalog #420201), pelleted at 300 × *g* for 5 min, resuspended in 200 µl of cell staining buffer, and fixed with 0.4% PFA in PBS. Data were acquired with the YETI Cell Analyzer (Propel Labs) using Everest Software (Bio-Rad Laboratories). Gating strategy and raw flow cytometry data were analyzed using FlowJo software version 10.6.1 (TreeStar). Cell gating was initially set using forward-scatter versus side-scatter plots of all events that corresponded to the size of cells. These cells were gated and labeled "blood cells." These cells were then gated using the Live/Dead stain, gating for live cells only. Live cells were then gated for singlets (single-cell events) by comparing forward-scatter width and side-scatter area. Singlets were then analyzed for the presence of leukocytes using CD45 expression. $CD45^+$ cells were then further analyzed for myeloid lineage cells using CD11b. Granulocyte cells were excluded by gating $CD45^+$ $CD11b^+$ $CD3^+$ cells. T- and B-cells were analyzed using CD3 and C19 expression, respectively. Finally, macrophages were analyzed by the endogenous GFP expression.

Cochlear protein lysates

Following perfusion with ice-cold PBS (Fisher Scientific, catalog #BP661-10), temporal bones were excised and placed in PBS containing 0.01% protease and phosphatase inhibitor (Thermo Scientific, catalog #78441). The stapedial artery, local bone marrow niche, and vestibule were removed. Isolated and pooled cochleae were crushed using Eppendorf mortar (Funakoshi, NIP-8913-00) in 100 µl of lysis buffer (Fisher Scientific, catalog #EPX-9999-000) using Eppendorf motor (Funakoshi, catalog #891-300) for 30 s twice on ice. Supernatant was collected after centrifugation at 12,000 × *g* for 10 min at cold conditions (Eppendorf centrifuge, 5804). Cochlear protein lysates were aliquoted and stored at −80°C until further used for multiplex Luminex assay for measuring cytokine and chemokine levels. Protein concentration was estimated using a BCA kit (Fisher Scientific, Reagent A catalog #23228, Reagent B 1859078), following the manufacturer's protocol against the BSA standard (Fisher Scientific, catalog #23209).

Luminex assay

Luminex assay was performed to detect the protein levels of various cytokines and chemokines in cochlear protein lysates using a custom-built multiplex panel as per the manufacturer's protocol (Fisher Scientific, catalog #PPX-26-MXPRMA9). Briefly, magnetic beads coated with target antibodies were added to the 96-well assay plate and washed 3 times with wash buffer. Standards for 26 cytokine and chemokine analytes were mixed and serially diluted to generate standard curves. Cochlear protein lysates at a concentration of 60 µg were used. Antigen standards, blanks, sample lysates were incubated with magnetic beads at room temperature at 500 rpm for 120 min in the dark. Then beads were washed 3 times to remove the excess lysate/standard; 25 µl of detection antibody was added and incubated in the dark for 30 min at room temperature. The beads were washed 3 times; 50 µl of streptavidin-PE was added and incubated for 30 min in the dark at room temperature. Washed beads were resuspended in 120 µl of reading buffer, and the plate was read using a Luminex 100/200 system (Fisher Scientific, FLEXMAP 3D). Acquired raw data were analyzed using 5PL algorithm offered by Fisher Scientific (Procartaplex Analysis App available online). Raw data files from the instrument were fed in the application, and the lot numbers of standards were entered. By following the manufacturer's instructions, the application

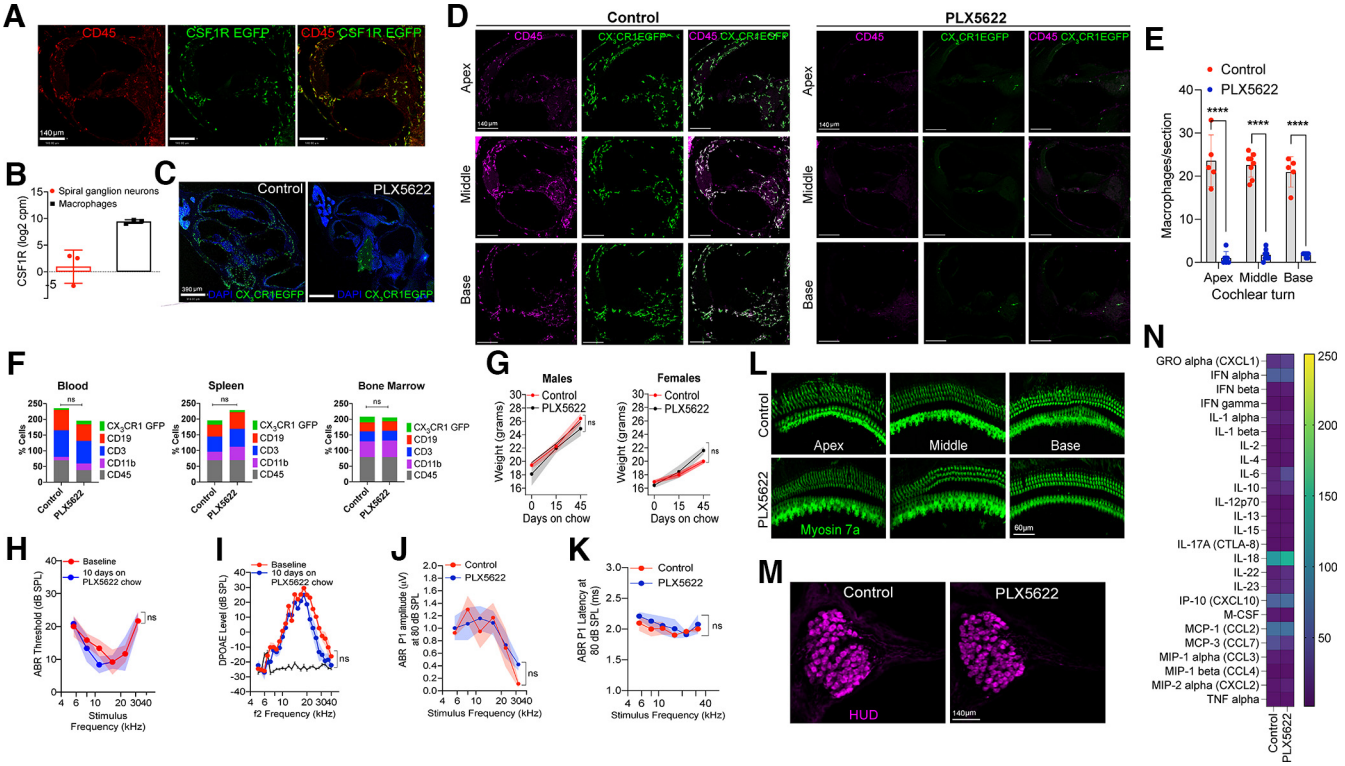

Figure 1. Selective CSF1R oral inhibitor PLX5622-induced ablation of resident cochlear macrophages. ***A***, Cochlear middle turn of mature *CSF1R-EGFP* mice shows that CSF1R (green) is expressed exclusively on CD45 (red) immunolabeled macrophages. Scale bars, 140 μm. ***B***, *CSF1R* transcripts in mature cochlear macrophages and SGNs. cpm, counts per million. Three independent experiments. ***C***, Cochlear mid-modiolar cross-sections from mature *CX_3CR1-EGFP* mice fed on control or PLX5622 chow for 10 d. Right, Green cells are the CX_3CR1-EGFP-positive macrophages in the cochlear nerve that are unaffected by PLX5622 chow treatment. Scale bar, 390 μm. ***D***, Cochlear cross-sections immunolabeled for CD45 leukocytes (magenta) and GFP macrophages (green) from apex, middle, and basal turns of mature *CX_3CR1-EGFP* mice fed on control or PLX5622 chow for 10 d. Scale bars, 140 μm. ***E***, Numbers of macrophages per section in cochlear apex, middle, and base turns ($n = 2$ cochleae from 2 mice per chow as well as 7 and 8 sections per cochlea). ****$p < 0.001$; two-way ANOVA, Sidak's multiple comparisons test. ***F***, Immune cell profile of blood, spleen, and bone marrow of mature *CX_3CR1-EGFP* mice fed on control or PLX5622 chow for 30 d (3 mice per chow). ***G***, Body weight of male ($n = 4$-6 mice) and female ($n = 6$ or 7 mice) mature *CX_3CR1-EGFP* mice fed on either control or PLX5622 chow for 45 d. ***H***, ABR thresholds of *CX_3CR1-EGFP* mice fed on PLX5622 chow for 10 d ($n = 6$ mice). ***I***, DPOAE levels of *CX_3CR1-EGFP* mice fed on PLX5622 chow for 10 d ($n = 6$ mice). Black solid line indicates noise floor. ABR Peak 1 (***J***) amplitudes and (***K***) latencies at 80 dB SPL across cochlear stimulus frequencies after 45 d on control or PLX5622 chow treatment ($n = 3$ or 4 mice). ***L***, Representative confocal images of cochlear whole mounts from apex, middle, and base regions showing intact Myosin 7a-immunolabeled IHCs and OHCs (green) after 45 d on control chow or PLX5622 chow. Scale bar, 60 μm. ***M***, Representative confocal images showing intact HUD-immunolabeled SGN cell bodies (magenta) in middle cochlear turn after 45 d on control chow or PLX5622 chow. Scale bar, 140 μm. ***N***, Multiplex Luminex-based cytokines, and chemokine profile of cochleae from mature *CX_3CR1-EGFP* mice fed on control or PLX5622 chow for 30 d (two independent replicates per chow). Data are mean ± SD. ns, not significant

computes the concentration and displays the graph for individual analytes.

Immunohistofluorescence

Cochlear microdissected whole mounts or frozen mid-modiolar cross sections (20-25 μm) were rinsed with PBS (Fisher Scientific, catalog #BP661-10) at least 3 times and incubated at room temperature for 2 h in blocking solution containing 5% normal horse serum (Sigma-Aldrich, catalog #H0146) in 0.2% Triton X-100 (Sigma-Aldrich, catalog #A16046AP) in PBS. For synaptic immunolabeling, cochlear microdissected whole mounts were incubated overnight at room temperature with combinations of the following primary antibodies: CtBP2 mouse (BD Biosciences, catalog #612044; RRID:AB_399431; 1:200), GluA3 goat (Santa Cruz Biotechnology, catalog #7612; RRID: AB_2113895; 1:50), or GluA2 mouse (EMD Millipore, catalog #AB1506; RRID:AB_11212990; 1:100), Myosin 7a rabbit (Proteus Biosciences, catalog #25-6790; RRID:AB_2314838; 1:500). For neuron and macrophage immunolabeling, cochlear frozen mid-modiolar cross sections were incubated overnight at room temperature with combinations of following primary antibodies: CD45 goat (R&D Systems, catalog #AF114; RRID:AB_442146; 1:50), anti-GFP (Invitrogen, catalog #A-11 122; RRID:AB_221569; 1:500, to enhance visualization of CSF1REGFP- or CX_3CR1GFP-expressing macrophages), Neurofilament 165 (NF-H) mouse (Developmental Studies Hybridoma Bank, catalog #2H3C, 1:100), and HUD mouse (Santa Cruz Biotechnology, catalog #sc-28 299; RRID:AB_627765; 1:100). Following incubation in primaries, specimens were rinsed 5 times in PBS and treated for 2 h at room temperature in species-specific secondary antibodies conjugated to either DyLight 405 (1:500, Jackson ImmunoResearch Laboratories) or AlexaFluor-488, -546, -555, or -647 (1:500; Invitrogen). Tissue was mounted in glycerol:PBS (9:1) and coverslipped before confocal imaging. Tissue samples were batch processed using the same reagent solutions in six cohorts, each including noise-exposed and sham-exposed control chow, PLX5622 chow, and PLX5622 to control chow fed mice.

Confocal imaging

Three- or four-color fluorescence imaging was performed using a Zeiss LSM 700 laser scanning confocal microscope (Carl Zeiss Microscopy 700). *Z*-series images using 10×, 20×, 40×, or 63× objectives were obtained. Image processing and quantitative analyses were performed using IMARIS (version 9.9.0, Oxford) and Volocity 3D image (version 6.5.1, PerkinElmer) software.

Synapse counts and volume measurements

Two or three confocal *z* stacks were obtained using a high-resolution oil immersion objective (63× with 1.4 numerical aperture) and a digital zoom of 1.5 from apical (5, 8, and 11 kHz), middle (16 and 22 kHz), and basal (32 and 45 kHz) regions per cochlear whole mount. Each *z* stack spanned the entire synaptic pole of 8-10 IHCs in the *z* dimensions, with *z* step size of 0.3 μm, from the apical portion of the IHC to nerve

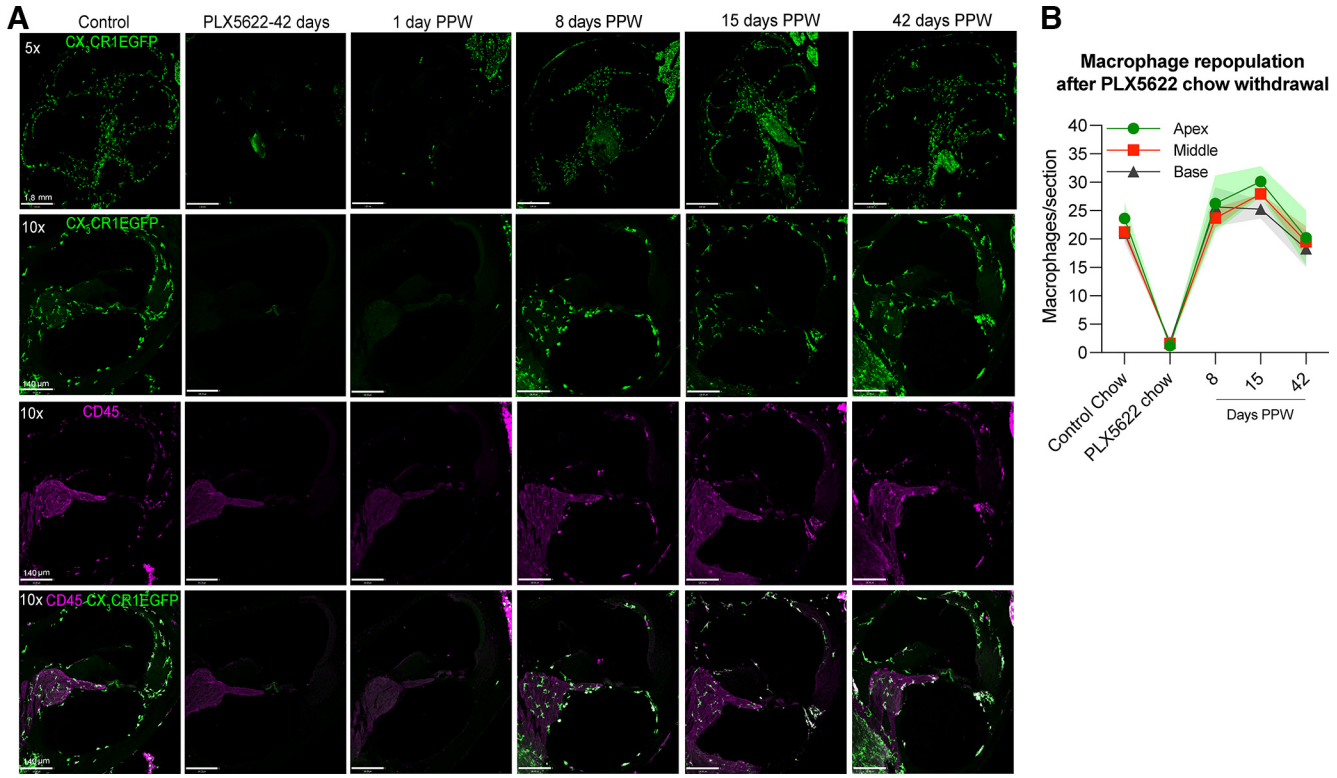

Figure 2. Rate and degree of macrophage repopulation in the cochlea after terminating PLX5622 treatment. ***A***, Mid-modiolar cochlear frozen sections double-immunolabeled for CX_3CR1-GFP macrophages (green) and CD45 leukocytes (magenta) showing the rate of repopulation of macrophages following removal of PLX5622 chow after 14 d of treatment and replacement with control chow. Scale bars: top (5×), 1.80 mm; bottom (10×), 140 µm. ***B***, Numbers of macrophages per cochlear turn per section at 14 d on control chow (baseline numbers), or PLX5622 chow or at 8, 15, 42 d PPW and replacement with control chow. The numbers of macrophages per cochlear section at 8, 15, and 42 d PPW are similar to the numbers in control chow in all cochlear turns. Two-way ANOVA, Tukey's multiple comparisons test. $n = 3$ cochleae from 3 mice per group or time point PPW. Data are mean ± SD.

terminal in the habenula perforata region. IMARIS was used for 3D analysis of juxtaposed/paired and orphan presynaptic and postsynaptic counts and volume. Thresholds for all the channels were adjusted in such a way the background is reduced without losing any prominent fluorescence and two close fluorescent punctae are not merged. For each paired synapse, overall volume (μm^3) was estimated as the volume of the surface created by the IMARIS for the virtual channels that is equal to the sum of either CtBP2 or GluA2 fluorescence. The paired CtBP2 and GluA2 fluorescence surface were counted as juxtaposed synapses. Total synaptic counts were divided by the number of surviving IHCs to report ribbon synapses per IHC. Any unpaired or orphan CtBP2 and GluA2 fluorescence was noted to compute the orphan presynaptic and postsynaptic punctae per IHC. For Figures 5 and 10, juxtaposed ribbon synapse density, orphan CtBP2 and GluA2 punctae per IHC, and median CtBP2 and GluA2 volume for paired synapses were averaged and plotted from the images taken from the middle cochlear region corresponding to 16-22 kHz.

SGN counts

SGN counts were analyzed at 30 DPNE to 93 dB SPL. To assess the numbers of SGN cell bodies, double NF-H (cytoplasmic) and HUD (nuclear) immunolabeled somata within Rosenthal's canal (spiral ganglion) were counted from the 3D projections of each section (20 µm thickness). HUD fluorescence spots were automatically quantified by IMARIS and cross-checked manually. SGN cell bodies from 7 or 8 sections per cochlea were normalized to the cross-sectional area of Rosenthal's canal per cochlear turn, averaged, and reported as SGN per mm^2 along the apical, middle, and basal cochlear regions.

Macrophage counts

CX_3CR1-GFP and CD45 double-labeled macrophages were counted in apical, middle, and basal cochlear regions or in the Rosenthal's canal or spiral ganglion from at least 7 or 8 mid-modiolar frozen sections (20 µm thickness) per cochlea. Following intensity thresholding, GFP fluorescence was automatically quantified by IMARIS, and macrophage numbers were cross-checked manually. Raw macrophage numbers in spiral ganglion were normalized to the cross-sectional area of the Rosenthal's canal of the respective cochlear region and averaged as macrophages in spiral ganglion (SG) per mm^2.

Statistical analyses

All statistical analyses were performed using Prism GraphPad version 9.1.2. Values are expressed as mean ± standard deviation (SD) across animals in each experimental group unless otherwise stated in the figure legends. Student's *t* test, or one- or two-way Analysis of variance (ANOVA), was applied as appropriate. Significant main effects or interactions were followed by appropriate *post hoc* tests. Details on error bars, statistical analysis, numbers of mice, and experimental replicates can be found in Results and figure legends. Results were considered statistically significant when probability (*p* values) of the appropriate statistical test was less than or equal to the significance level ($\alpha = 0.05$).

Results

CSF1R inhibition eliminates cochlear macrophages without affecting cochlear structure and function

To determine the precise role of macrophages in noise-induced synaptic degeneration and repair, resident cochlear macrophages were depleted using PLX5622, which is an orally available inhibitor of CSF1R. Using a CSF1R-EGFP transgenic mouse line, we first verified that expression of CSF1R in the mature cochlea is limited to macrophages (Fig. 1*A*,*B*). Mice that were fed on PLX5622-containing chow exhibited a nearly complete elimination of CX_3CR1-GFP-labeled resident macrophages by ~94% from all the turns in the cochlea (Fig. 1*C*–*E*). In contrast, PLX5622 did not significantly affect the percentage of different types of leukocytes in peripheral

blood ($p = 0.15$), spleen ($p = 0.14$), and bone marrow ($p = 0.64$) (Fig. 1*F*, two-way ANOVA), nor did it affect the mouse body weight during the experiment (Fig. 1*G*, $p = 0.70$ and $p > 0.99$ for males and females, respectively, Mann–Whitney test). Assessment of the gross cochlear function, and survival of sensory hair cells and SGNs also showed no significant changes in PLX5622-treated mice [Fig. 1*H–M*, $p = 0.27$ (Fig. 1*H*), $p = 0.20$ (Fig. 1*I*), paired *t* test and $p = 0.64$ (Fig. 1*J*), $p = 0.30$ (Fig. 1*K*), two-way ANOVA]. To determine whether PLX5622-mediated macrophage ablation influenced the inflammatory profile in the uninjured cochlea, a Luminex-based multiplex cytokine and chemokine assay was performed on protein lysates extracted from the cochleae of *CX$_3$CR1-EGFP* mice, that were maintained for 30 d on either PLX5622-containing or control chow. No significant differences were observed in the expression levels of various inflammatory mediators between the two treatment groups (Fig. 1*N*, $p = 0.37$, two-way ANOVA). Together, the data indicate that CSF1R inhibition via PLX5622 chow is an effective tool for sustained depletion of resident cochlear macrophages without affecting the peripheral immune cells, cochlear function, structure, or inflammation.

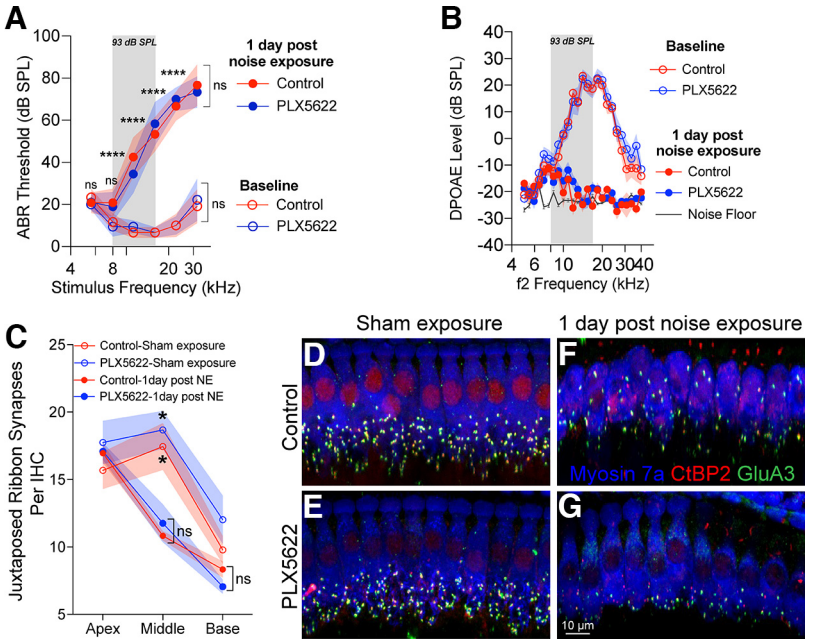

Figure 3. Cochlear function and IHC ribbon synapse density at 1 DPNE in the presence or absence of resident macrophages. ***A***, ABR thresholds of adult *CX$_3$CR1-EGFP* mice fed on control ($n = 5$ mice) and PLX5622 ($n = 7$ mice) chow for 14 d at baseline and 1 DPNE for 2 h at 93 dB SPL. Gray bar represents the noise band of 8-16 kHz. ****$p <$ 0.0001, baseline versus 1 DPNE at respective stimulus frequencies, control versus PLX5622, two-way ANOVA, ***B***, DPOAE levels of adult *CX$_3$CR1-EGFP* mice fed on control ($n = 5$ mice) and PLX5622 ($n = 7$ mice) chows for 14 d at baseline and 1 DPNE for 2 h at 93 dB SPL. Black line indicates noise floor. ***C***, Juxtaposed ribbon synapse density per IHC in apex (5, 8, and 11 kHz), middle (16 and 22 kHz), and base (32 and 45 kHz) regions of the cochlea of mature *CX$_3$CR1-EGFP* mice fed on control ($n = 3$-5 cochleae from 3-5 mice) and PLX5662 ($n = 3$-5 cochleae from 3-5 mice) chows for 14 d after sham exposure or at 1 DPNE. *$p < 0.05$, sham exposure versus 1 DPNE in middle cochlear turn; control versus PLX5622, two-way ANOVA, Tukey's multiple comparisons test. ***D–G***, Representative confocal images showing IHC ribbon synapses in middle region of the cochlea from adult *CX$_3$CR1-EGFP* mice fed on control and PLX5622 chows for 14 d after sham exposure or at 1 d after noise. Scale bar, 10 µm. Data are mean ± SD. ns, not significant.

Macrophages repopulate the cochlea after terminating PLX5622 treatment

Next, we examined the rate and degree of macrophage repopulation in the cochleae of PLX5622-fed mice, once PLX5622 treatment was terminated. After 14 d of continuous PLX5622 treatment, the PLX5622 chow was removed and replaced with control chow to allow macrophage repopulation. Cochleae were excised at 1, 8, 15, and 42 d post PLX5622 chow withdrawal (PPW) and processed for visualization and quantification of macrophages. By 8 d PPW, macrophages had repopulated the entire cochlea and expressed both CD45 and CX$_3$CR1-EGFP (Fig. 2*A*). The numbers of macrophages at 8 and 15 d PPW were comparable to the numbers of resident macrophages at baseline (control chow) and remained unchanged up to 42 d PPW in all the turns of the cochlea (Fig. 2*B*, $p < 0.0001$ for control chow vs PLX5622 chow and PLX5622 chow vs 8, 15, and 42 d PPW for apex, middle, and base; $p = 0.91$, 0.25, and 0.81 for control chow vs 8, 15, and 42 d PPW, respectively, in apex; $p = 0.93$, 0.22, and 0.98 for control chow vs 8, 15, and 42 d PPW, respectively, in middle; $p = 0.58$, 0.66, and 0.90 for control chow vs 8, 15, and 42 d PPW, respectively, in base; two-way ANOVA, Tukey's multiple comparison test). Hence, the depletion of resident cochlear macrophages is sustained in the presence of PLX5622, but is reversible once CSF1R inhibition is removed.

Macrophages do not affect the loss of IHC ribbon synapses at 1 DPNE

Previously, we had shown that, immediately after synaptopathic noise exposure, macrophages migrate toward the damaged IHC-synaptic region and directly contact the damaged synaptic connections (Kaur et al., 2019). Adult *CX$_3$CR1-EGFP* mice were continuously maintained on either control or PLX5622 chow for 2 weeks, and then exposed for 2 h exposure to an octave band noise (8-16 kHz) at 93 dB SPL. Cochleae were harvested at 1 d after exposure, the time point of maximum damage or loss of IHC ribbon synapses (Kaur et al., 2019), to examine whether the absence of macrophages affected the loss of IHC ribbon synapses after noise exposure. Auditory functional assessment at 1 DPNE showed a significant elevation in ABR thresholds ranging from ~10 to 65 dB at 8, 11.2, 16, 22.6, and 32 kHz test frequencies (Fig. 3*A*) and a reduction in DPOAE levels up to the noise floor (Fig. 3*B*) in both control and PLX5622-fed mice compared with sham-exposed mice. The mean differences in ABR thresholds and DPOAE levels between the two groups at 1 DPNE were nonsignificant at all test frequencies (Fig. 3*A*,*B*, $p = 0.63$ [Fig. 3*A*], $p = 0.67$ [Fig. 3*B*], two-way ANOVA). Examination of the mean number of juxtaposed ribbon synapses per IHC revealed a significant ~40% loss of synapses in the middle (16-22 kHz) region of the cochleae of noise-exposed control and PLX5622 group compared with sham-exposed groups ($p = 0.01$, control and $p = 0.01$, PLX5622, two-way ANOVA). At 1 DPNE, the average synapse loss per IHC in the middle region of the cochlea in exposed control and PLX5622 group was 10.8 and 11.7, which was statistically insignificant between the two groups ($p = 0.97$, two-way ANOVA) (Fig. 3*C–G*). A mild but insignificant loss of synapses also occurred in the basal (32-45 kHz) region of the cochlea after noise exposure ($p = 0.89$, control and $p = 0.10$, PLX5622, two-way ANOVA). However, no significant difference in the mean numbers of paired synapses per IHC in the basal cochlear region was

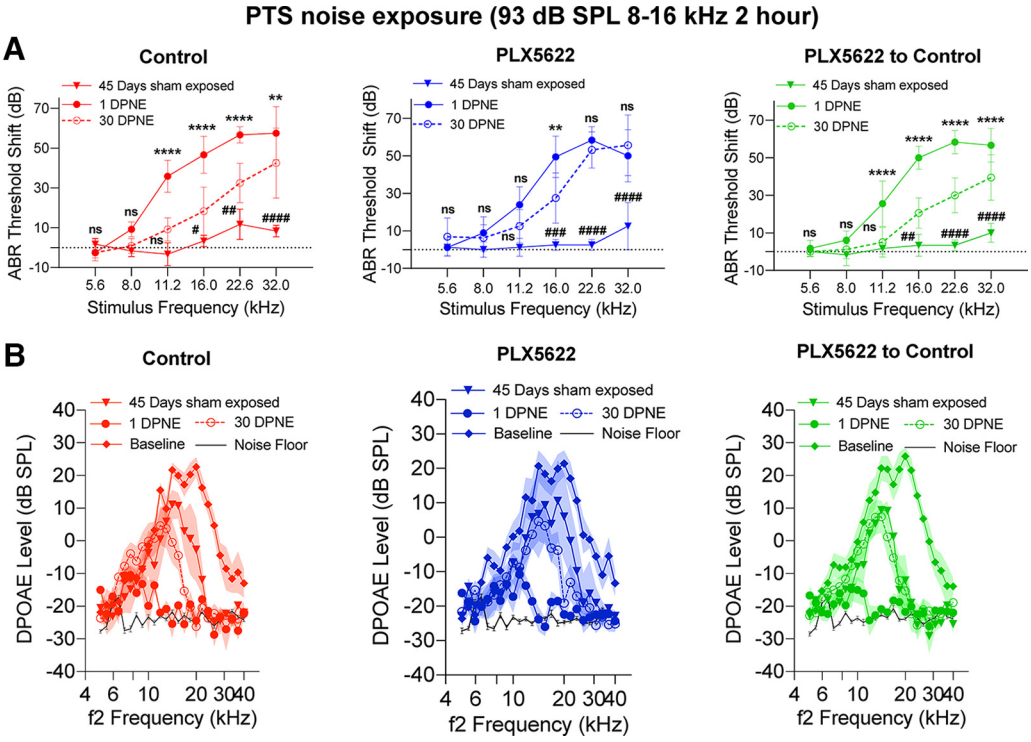

Figure 4. Cochlear function at 1 and 30 d after exposure to PTS-imparting 93 dB SPL noise level in the presence, absence, or repopulated macrophages. ***A***, ABR threshold shifts at 1 and 30 DPNE at 93 dB SPL (8-16 kHz) for 2 h. Control chow ($n = 6$ mice), PLX5622 chow ($n = 9$ mice), and PLX5622 chow replaced with control chow ($n = 9$ mice). *Comparison between 1 and 30 DPNE: $^{**}p < 0.01$; $^{****}p < 0.0001$; respective stimulus frequencies. $^{\#}$Comparison between 30 DPNE and 45 d sham-exposed: $^{\#}p < 0.05$; $^{\#\#}p < 0.01$; $^{\#\#\#\#}p < 0.0001$; two-way ANOVA, Sidak's multiple comparisons test. For 45 d on chow sham exposure, ABR threshold shifts, control chow ($n = 3$ mice), PLX5622 chow ($n = 4$ mice), and PLX5622 chow replaced with control chow ($n = 3$ mice). Dashed line indicates threshold shifts at baseline (prenoise exposure). Dotted line indicates threshold shifts at baseline (prenoise exposure). ***B***, DPOAE levels at baseline (pre-chow), 1 DPNE, 30 DPNE at 93 dB SPL (8-16 kHz) for 2 h and of age-matched sham-exposed mice after 45 d fed on control chow ($n = 6$ mice), PLX5622 chow ($n = 9$ mice), and PLX5622 chow replaced with control chow ($n = 9$ mice) chows. For 45 d on chow sham exposure, DPOAE levels, control chow ($n = 3$ mice), PLX5622 chow ($n = 4$ mice), and PLX5622 chow replaced with control chow ($n = 3$ mice). Black line indicates noise floor. Data are mean ± SD. ns, not significant.

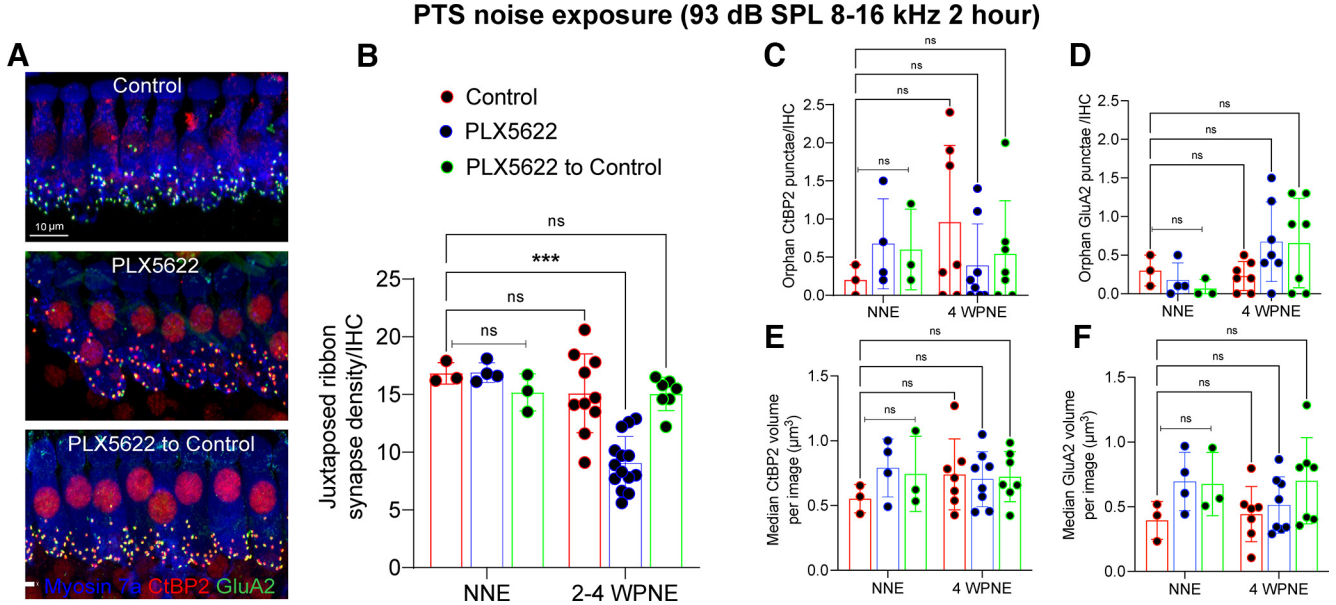

Figure 5. Repair of IHC ribbon synapses in the presence, absence, or repopulated macrophages at 2-4 weeks after 2 h of exposure at 93 dB SPL noise level. ***A***, Representative confocal images showing juxtaposed IHC ribbon synapses in middle cochlear region (16-22 kHz) at 4 weeks after noise exposure. Scale bar, 10 µm ***B***, Juxtaposed ribbon synapse density per IHC. $^{***}p <$ 0.001; two-way ANOVA, Tukey's multiple comparisons test. ***C***, Orphan CtBP2 presynaptic punctae per IHC. ***D***, Orphan GluA2 postsynaptic punctae per IHC. ***E***, Median CtBP2 volume of paired synapses. ***F***, Median GluA2 volume of paired synapses. For no noise exposure (NNE), $n = 3$ cochleae from 3 mice (control), $n = 4$ cochleae from 4 mice (PLX6522), and $n = 4$ cochlea from 4 mice (PLX5622 to control). For 2-4 weeks after noise exposure (WPNE), $n = 7$-10 cochleae from 7-10 mice (control), $n = 7$-14 cochleae from 7-14 mice (PLX6522), and $n = 7$ cochleae from 7 mice (PLX5622 to control). Data are mean ± SD (***B–D***), median ± SD (***E***,***F***). ns, not significant.

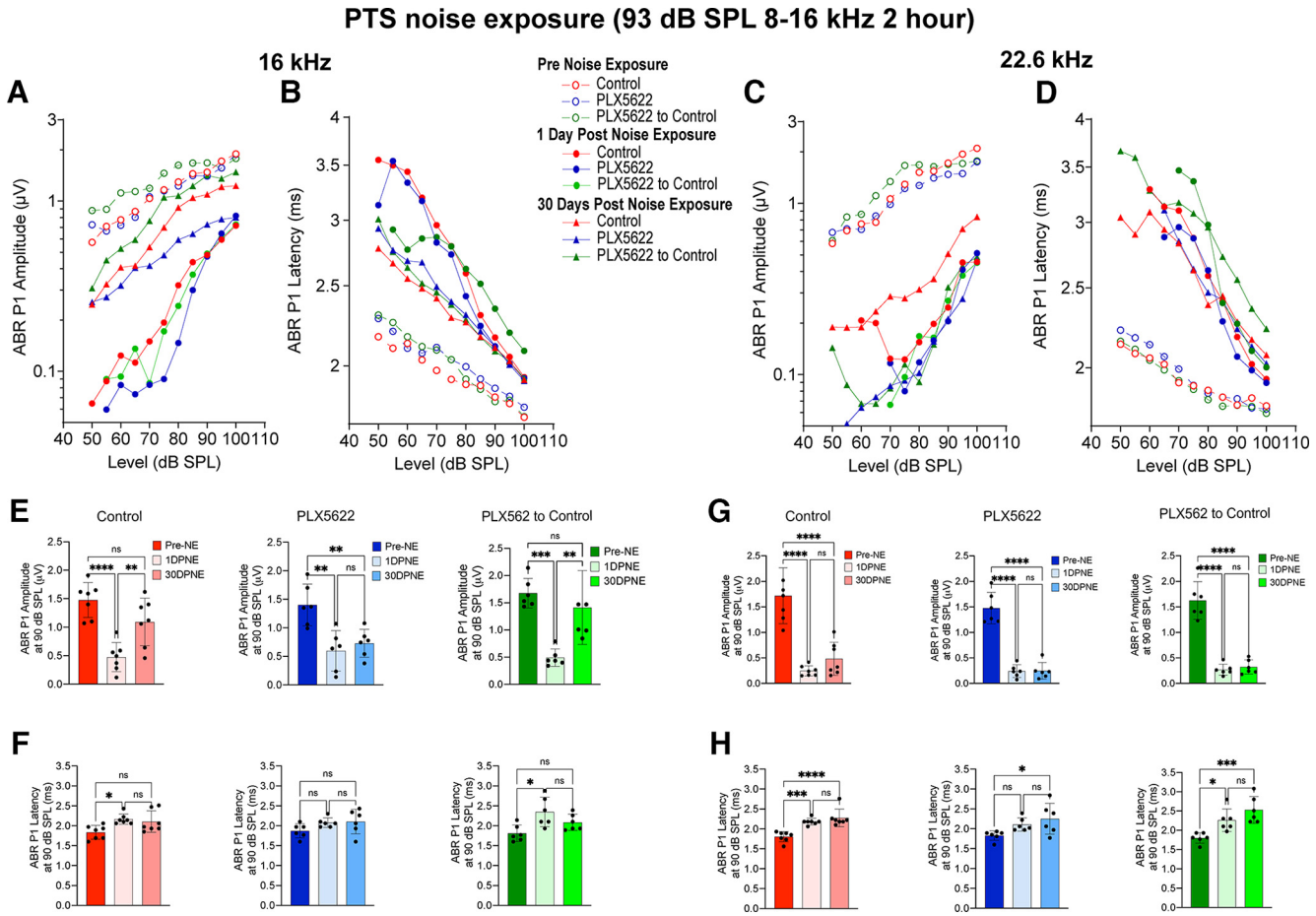

Figure 6. ABR Peak 1 I/O function and suprathreshold amplitude and latency in the presence, absence, or repopulated macrophages at 16 and 22.6 kHz after exposure at 93 dB SPL noise level. ***A***, ABR Peak 1 (P1) amplitude and (***B***) latency I/O function at 16 kHz at baseline (pre-NE), 1 DPNE, and 30 DPNE. ***C***, ABR Peak 1 amplitude and (***D***) latency I/O function at 22.6 kHz at baseline (pre-NE), 1 DPNE, and 30 DPNE. ***E***, ABR Peak 1 amplitude and (***F***) latency at suprathreshold stimulus level at 16 kHz at baseline (pre-NE), 1 DPNE, and 30 DPNE. ***G***, ABR Peak 1 amplitude and (***H***) latency at suprathreshold stimulus level at 22.6 kHz at baseline (pre-NE), 1 DPNE, and 30 DPNE. Values are mean (***A–D***), mean ± SD (***E–H***). Control chow ($n = 7$ mice), PLX6522 chow ($n = 6$ mice), and PLX5622 chow replaced with control chow ($n = 6$ mice). *$p < 0.05$; **$p < 0.01$; ***$p < 0.001$; ****$p < 0.0001$; one-way ANOVA, Tukey's multiple comparisons test. ns, not significant.

detected between control and PLX5662 group at 1 d after exposure ($p = 0.94$, two-way ANOVA) (Fig. 3*C*). Synapses per IHC in the apical (5, 8, and 11 kHz) region of control and PLX5622 cochleae appeared unchanged in response to noise exposure ($p = 0.92$, control and $p = 0.98$, PLX5622, two-way ANOVA) (Fig. 3*C*). In summary, these data imply that macrophages do not influence the degree of hearing loss or IHC ribbon synapse loss following synaptopathic noise exposure.

Absence of macrophages impedes the recovery of ABR thresholds after noise exposure

Having shown that PLX5622 greatly reduces the numbers of cochlear macrophages and does not alter the degree of hearing loss after a moderate noise exposure, we then sought to determine whether continued PLX5622 treatment affected the recovery of cochlear function after synaptopathic noise trauma. Age-matched sham-exposed mice fed on control, PLX5622, or PLX5622 to control chows for 45 d did not show any significant change in ABR thresholds compared with the baseline thresholds that were measured before starting the chows ($p = 0.17$, two-way ANOVA). At 1 DPNE, the magnitude of increase in ABR thresholds (i.e., ranging from ~5 to 60 dB across the test frequencies) was comparable between the three experimental groups ($p = 0.49$, two-way ANOVA) (Fig. 4*A*). By 30 d following noise exposure, the elevated ABR thresholds partially recovered close to baseline thresholds at ≥11.2 kHz stimulus frequencies in mice continuously maintained on control chow (Fig. 4*A*, right). Unexpectedly, such partial recovery of elevated ABR thresholds was not detected in mice that were continuously fed on PLX5622 chow (Fig. 4*A*, middle). Specifically, the thresholds at 30 d after exposure at 22.6, and 32 kHz test frequencies remained elevated at ~50 dB compared with thresholds at 1 DPNE. Remarkably, we observed similar partial recovery of the elevated ABR thresholds in mice that were initially fed with PLX5622 chow before noise exposure and returned to control chow after noise exposure (PLX5622 to control) (Fig. 4*A*, left). While the elevated ABR thresholds partially recovered in control and PLX5622 to control groups, the mean thresholds remained significantly higher than those of the sham-exposed age-matched mice at ≥16 kHz (Fig. 4*A*). In addition, DPOAE levels were significantly reduced at 1 DPNE compared with baseline levels but had nearly recovered by 30 d after exposure to similar levels as that of the age-matched sham-exposed mice ($p < 0.0001$ baseline vs 1DPNE [in all three groups]; $p = 0.55$ [control chow], $p = 0.31$ [PLX5622 chow], $p = 0.67$ [PLX5622 to control chow], 30 DPNE vs 45 d sham-exposed, two-way ANOVA, Tukey's multiple comparison test) (Fig. 4*B*). Moreover, no significant outer hair cell (OHC) or IHC loss was observed in the three experimental group after such

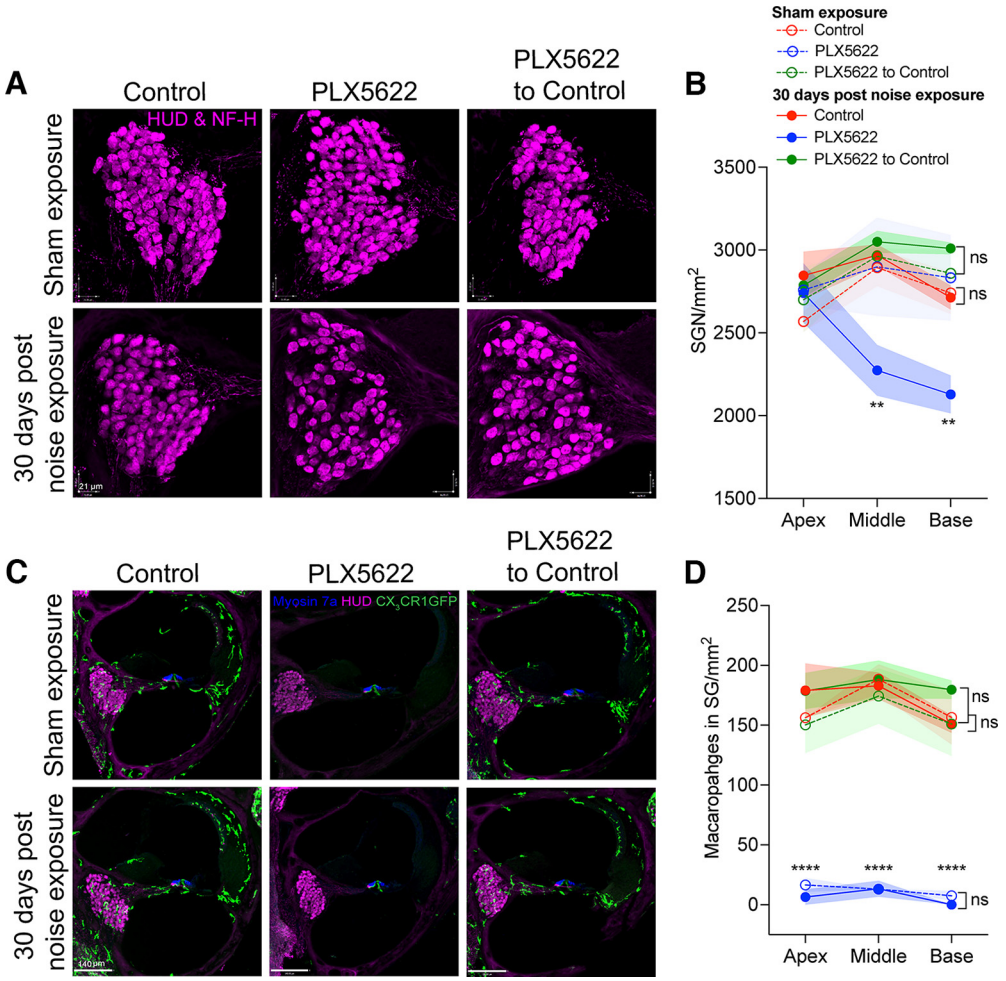

Figure 7. Densities of neuronal cell bodies and macrophages in spiral ganglion in the presence, absence, or repopulated macrophages at 30 d after exposure at 93 dB SPL noise level. ***A***, Representative confocal images of HUD and NF-H double-positive SGN cell bodies in middle cochlear turn from age-matched sham-exposed and 30 d noise-exposed mice fed on control chow, PLX5622 chow, and PLX5622 chow replaced with control chow. Scale bar, 21 µm. ***B***, SGN density per mm^2. **$p < 0.01$; sham-exposed versus noise-exposed PLX5622; sham-exposed versus noise-exposed control or PLX5622 to control, two-way ANOVA, Tukey's multiple comparisons test. ***C***, Cochlear middle turn showing CX_3CR1-GFP macrophages (green) from age-matched sham-exposed and 30 DPNE mice fed on control chow, PLX5622 chow, and PLX5622 chow replaced with control chow. Scale bar, 140 µm. ***D***, Density of macrophages in spiral ganglion per mm^2. ****$p <$ 0.0001; sham and noise-exposed PLX5622 versus sham and noise-exposed control or PLX5622 to control; sham-exposed versus noise-exposed control, PLX5622, or PLX5622 to control, two-way ANOVA, Tukey's multiple comparisons test. For sham exposure, control ($n = 3$ cochleae from 3 mice), PLX5622 ($n = 3$ cochleae from 3 mice), and PLX5622 to control ($n = 3$ cochleae from 3 mice). For 30 DPNE, control ($n = 3$ cochleae from 3 mice), PLX5622 ($n = 5$ cochleae from 5 mice), and PLX5622 to control ($n = 5$ cochleae from 5 mice). Data are mean ± SD. ns, not significant.

synaptopathic noise injury (data not shown). Together, these functional data suggest that macrophages may serve as critical mediators of partial recovery from an acute moderate PTS-imparting noise-induced hearing loss.

Macrophages promote repair of damaged IHC ribbon synapses after noise exposure

Data presented above indicate that macrophages do not influence the damage or loss of IHC ribbon synapses at 1 DPNE. We next sought to determine whether macrophages promote the repair of ribbon synapses after noise injury. We quantified paired or juxtaposed synapses per IHC in the middle region of the cochlea (where we observed significant synaptic loss after noise exposure, see Fig. 3*C*,*D*) at 2-4 weeks after noise exposure. Although synapse loss in control and PLX5622 group was similar at 1 d after exposure, recovery of juxtaposed ribbon synapses per IHC was greater at 2-4 weeks recovery in mice that were fed control chow, than in mice that were maintained for the entire period on PLX5622-containing chow. Notably, PLX5622-fed mice that were returned to control chow immediately after noise exposure (thereby permitting macrophage recovery) also displayed significant synapse repair (Fig. 5*A*). After 2-4 weeks recovery, the cochleae of exposed control mice and of PLX5622-fed mice that were returned to control chow after noise exposure possessed on average 15.09 ± 3.4 and 15.04 ± 1.44 synapses per IHC, respectively, which were not significantly different from the number of synapses per IHC in the sham-exposed age-matched mice on the respective chows, that is, 16.83 ± 0.92 and 15.16 ± 1.60 ($p = 0.99$ and 0.99, two-way ANOVA). In contrast, mice that were fed PLX5622-containing chow for the entire duration of the experiment showed no evidence for repair of synapses and the cochleae of these mice possessed 9.04 ± 2.3 synapses per IHC, which is significantly different from sham- and noise-exposed mice fed on control chow and of PLX5622-fed mice that were returned to control chow ($p \leq 0.0001$, two-way ANOVA) (Fig. 5*B*). While there was an insignificant IHC synaptic loss in the basal region of the cochleae at 1 DPNE in control chow and PLX5622 chow treatment groups, there was no evidence for synaptic repair in the basal region of the cochlea of mice that were fed PLX5622-containing chow for the entire duration of the experiment and

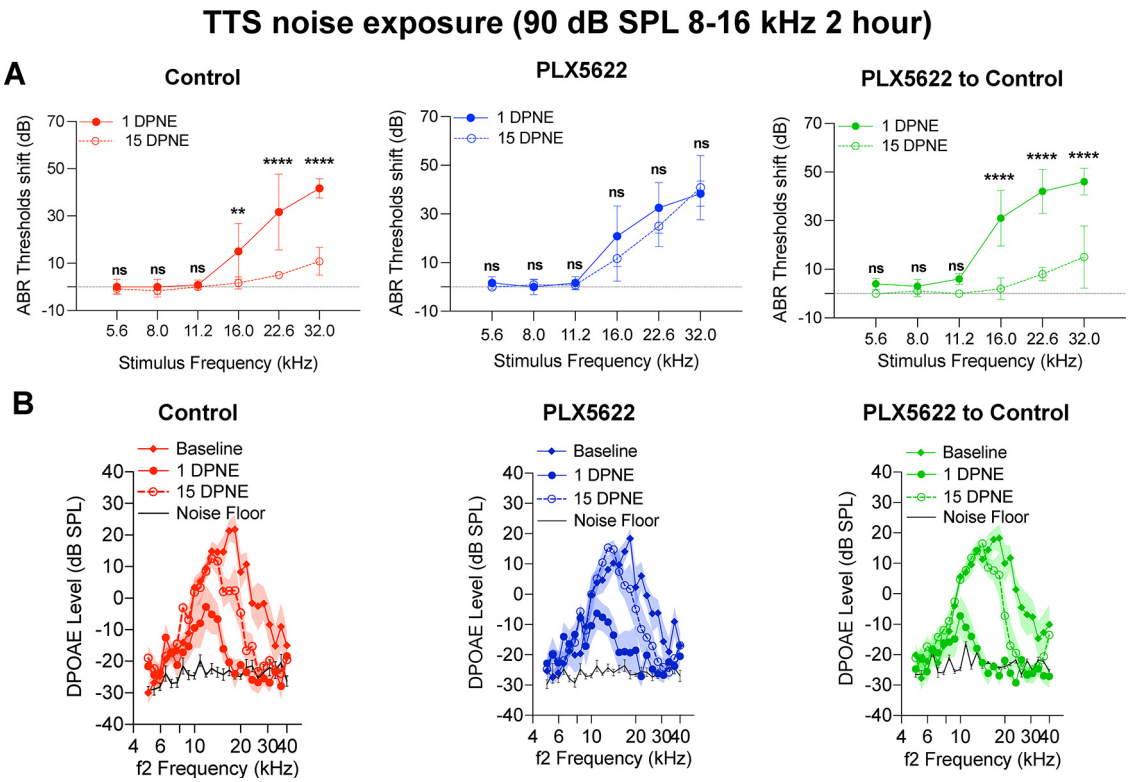

Figure 8. Cochlear function at 1 and 15 d after exposure to a TTS-imparting 90 dB SPL noise level in the presence, absence, or repopulated macrophages. ***A***, ABR threshold shifts at 1 and 15 DPNE of 2 h at 90 dB SPL at 8-16 kHz. Control chow ($n = 6$ mice), PLX5622 chow ($n = 6$ mice), and PLX5622 chow replaced with control chow ($n = 5$ mice). $^{**}p < 0.01$; $^{****}p < 0.0001$; comparison between 1 and 15 DPNE (two-way ANOVA, Sidak's multiple comparisons test). Dotted line indicates threshold shifts at baseline (prenoise exposure). ***B***, DPOAE levels at baseline (Pre-chow), 1 DPNE, and 15 DPNE of 2 h at 90 dB SPL at 8-16 kHz. Control chow ($n = 6$ mice), PLX5622 chow ($n = 6$ mice), and PLX5622 chow replaced with control chow ($n = 5$ mice). Black line indicates noise floor. Data are mean ± SD. ns, not significant.

the cochleae of these mice possessed 7.34 ± 1.2 synapses per IHC. On the other hand, mice fed on control chow or PLX5622 chow that were returned to control chow after noise exposure showed modest synaptic repair in the basal region and the cochlea of these mice possessed 10.33 ± 4.3 and 11.10 ± 3.6 synapses per IHC, respectively (data not plotted). No significant difference was detected in the densities of orphan CtBP2 and GluA2 punctae per IHC (Fig. 5*C*,*D*) or in the CtBP2 or GluA2 volumes for the paired synapses in the middle cochlear region (16-22 kHz) (Fig. 5*E*,*F*) between the three experimental groups either with no noise exposure or at 4 weeks after noise exposure. Together, these data suggest that cochlear macrophages restore noise-damaged IHC ribbon synapses.

Macrophages-mediated IHC synaptic repair positively correlates with recovery of ABR Peak 1 amplitudes after noise exposure

To determine whether macrophage-induced structural repair of ribbon synapses in the middle region of the cochlea correlates with functional synaptic recovery, we measured the ABR Peak 1 amplitude and latency at 16 and 22.6 kHz (similar midcochlear regions where synaptic damage and repair is detected) at baseline, 1 and 30 d after exposure to 93 dB SPL octave (8-16 kHz) band noise. At 16 kHz, the ABR Peak 1 amplitude was reduced at 1 d after exposure, which partially restored in macrophage-containing cochleae (i.e., control and PLX5622 to control groups) after 30 d recovery. However, recovery of Peak 1 amplitude was not detected in mice that were continuously maintained on PLX5622 chow (Fig. 6*A*,*E*). At 22.6 kHz, ABR Peak 1 amplitude was significantly reduced at 1 d after exposure, but no recovery was detected in any of the three experimental groups (Fig. 6*C*,*G*). ABR Peak 1 latency was increased at both 16 and 22.6 kHz after 1 d of noise exposure, that remained prolonged by 30 d recovery in all three experimental groups (Fig. 6*B*,*D*,*F*,*H*). From these data, we conclude that cochlear macrophage-mediated structural IHC synaptic repair partially correlates with functional recovery of diminished ABR Peak 1 amplitudes after synaptopathic noise exposure.

Macrophages promote the survival of SGNs after noise exposure

We next examined whether the presence of macrophages affected the survival of SGNs and whether the lack of synaptic repair in the absence of macrophages resulted in gradual loss of SGNs after exposure to PTS-imparting noise (93 dB SPL). No significant changes in the SGN density were observed in age-matched sham-exposed mice that were fed with control chow, PLX5622 chow, or PLX5622 to control chow for 45 d (Fig. 7*A*,*B*) ($p = 0.99$, two-way ANOVA). However, at 30 DPNE, there was ~22%-25% loss of SGN cell bodies in the middle and basal regions of the cochlea in the absence of resident cochlear macrophages. Cochleae with original resident or repopulated macrophages displayed preservation of neuron cell bodies (Fig. 7*A*,*B*). Noise-exposed cochleae deficient of macrophages displayed a significant SGN loss in the middle and basal regions compared with sham-exposed cochleae deficient of macrophages ($p = 0.003$ and $p = 0.008$, respectively, two-way ANOVA). The mean SGN density in sham and noise-exposed cochleae with resident or repopulated macrophages was similar in all cochlear regions:

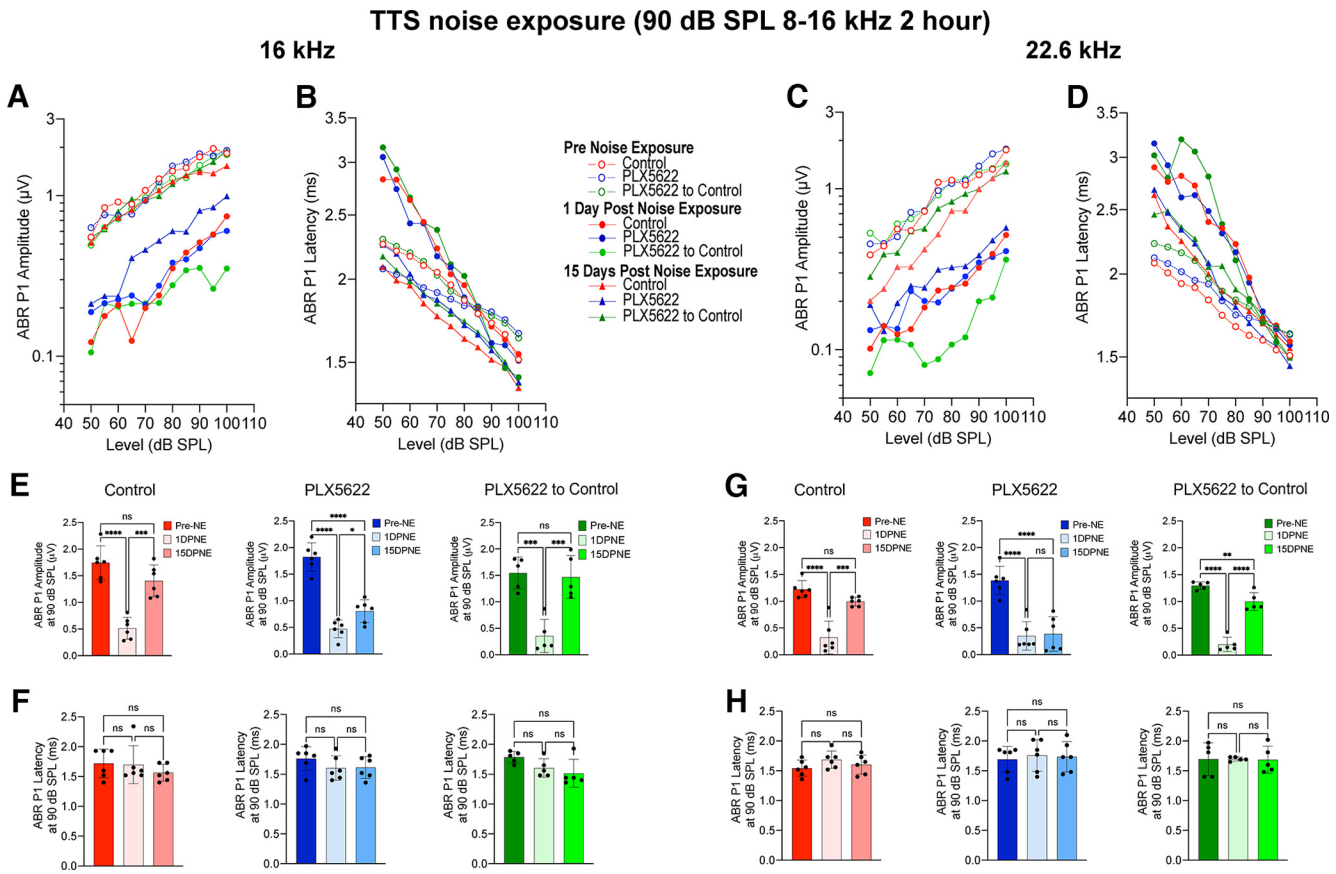

Figure 9. ABR Peak 1 I/O function and suprathreshold amplitude and latency in the presence, absence, or repopulated macrophages at 16 and 22.6 kHz after exposure at 90 dB SPL noise level. ***A***, ABR Peak 1 (P1) amplitude and (***B***) latency I/O function at 16 kHz at baseline (pre-NE), 1 d, and 15 DPNE. ***C***, ABR Peak 1 amplitude and (***D***) latency I/O function at 22.6 kHz at baseline (pre-NE), 1 DPNE, and 30 DPNE. ***E***, ABR Peak 1 amplitude and (***F***) latency at suprathreshold stimulus level at 16 kHz at baseline (pre-NE), 1 DPNE, and 30 DPNE. ***G***, ABR Peak 1 amplitude and (***H***) latency at suprathreshold level at 22.6 kHz at baseline (pre-NE), 1 DPNE, and 15 DPNE. Values are mean (***A–D***), mean ± SD (***E–H***). Control chow ($n = 6$ cochleae), PLX6522 chow ($n = 6$ cochleae), and PLX5622 chow replaced with control chow ($n = 5$ cochleae). *$p < 0.05$; **$p < 0.01$; ***$p < 0.001$; ****$p < 0.0001$; one-way ANOVA, Tukey's multiple comparisons test. ns, not significant.

$p = 0.86$ (apex), 0.96 (middle), and 0.73 (base), two-way ANOVA.

We next examined whether exposure to PTS-imparting noise level of 93 dB SPL affects macrophage numbers in the spiral ganglion of mice that were fed with control chow, PLX5622 chow, or PLX5622 to control chow. Macrophage numbers in the spiral ganglion in all cochlear regions were comparable between sham-exposed and 30 d after noise-exposed mice that were fed with control chow, PLX5622 chow, or PLX5622 to control chow (Fig. 7*C*,*D*) ($p = 0.98$, two-way ANOVA). Similarly, the macrophage density in spiral ganglion between the control and PLX5622 to control experimental groups was comparable in sham-exposed and 30 d noise-exposed mice (Fig. 7*C*,*D*) ($p > 0.05$, two-way ANOVA). Notably, continuous treatment with PLX5622 chow for 45 d maintained the absence of cochlear macrophages in both sham-exposed and noise-exposed mice. Moreover, such moderate PTS-like noise exposure (93 dB SPL for 2 h) did not significantly increase macrophage numbers in the spiral ganglion in all the three experimental groups when examined at 30 d (Fig. 7*D*) or 7 DPNE (data not shown). Together, these data reveal that macrophages play a critical neuroprotective role in moderate PTS exposures by preserving the SGN cell bodies, while their absence results in a significant loss of SGNs after noise injury that may be attributed to the IHC synaptic loss or impeded synaptic recovery. In acute noise-damaged cochlea, the presence or absence of resident cochlear macrophages coincides with survival or loss of SGNs, respectively.

Absence of macrophages impedes the recovery of ABR thresholds and Peak 1 amplitudes after temporary threshold shift (TTS) exposure

Data shown above indicate that cochlear macrophages play a critical role in regulating the partial recovery of ABR thresholds and Peak 1 amplitudes following an acute moderate PTS-imparting noise exposure. Next, we examined whether PLX5622 treatment also affected the recovery of elevated ABR thresholds following an exposure to a noise level that causes TTSs. For this, mice in the same three treatments groups were exposed for 2 h to 8-16 kHz octave band noise at 90 dB SPL, and cochlear function was measured before noise exposure and at 1 and 15 DPNE (Kaur et al., 2019). As expected, at 1 DPNE, a significant elevation in ABR thresholds ranging from ~20 to 45 dB across the test frequencies of ≥16 kHz was observed in all the three experimental groups. The degree of elevation in ABR thresholds between the three treatment groups was comparable ($p = 0.97$, two-way ANOVA). By 15 d following noise exposure, the elevated ABR thresholds nearly completely recovered to baseline thresholds at all stimulus frequencies in the mice that were fed with control chow (Fig. 8*A*, left). However, such recovery of ABR thresholds was not observed in mice that were maintained on PLX5622 chow for the entire period of the experiment (Fig. 8*A*, middle). Specifically, at 15 d after exposure, the thresholds at 16, 22.6, and 32 kHz test frequencies remained elevated by 11.6, 25, and 40.8 dB, respectively, compared with baseline thresholds. Moreover, there was no difference in the

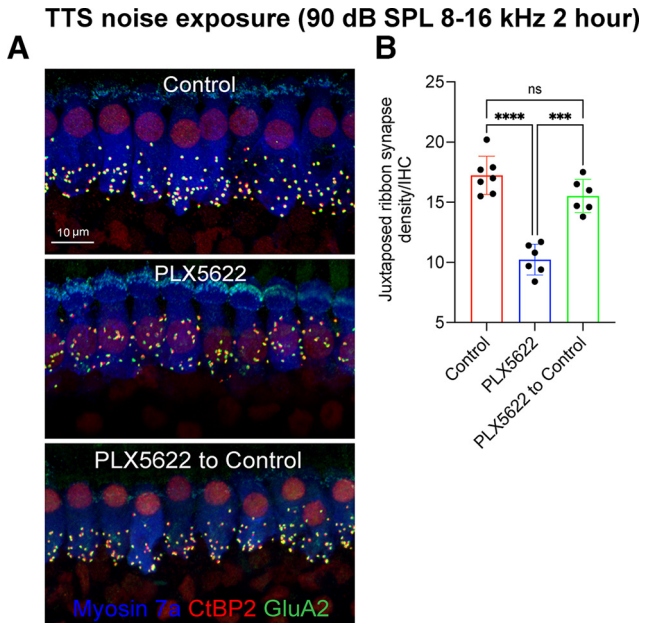

Figure 10. Repair of IHC ribbon synapses in the presence, absence, or repopulated macrophages at 4 weeks after 2 h of exposure at 90 dB SPL noise level. ***A***, Representative confocal images showing juxtaposed IHC ribbon synapses in midcochlear region at 4 weeks after TTS-inducing noise exposure from mice fed on control chow, PLX5622 chow, and PLX5622 chow returned to control chow. Scale bar, 10 µm. ***B***, Juxtaposed ribbon synapse density per IHC. Control chow ($n = 7$ cochleae from 7 mice), PLX6522 chow ($n = 6$ cochleae from 6 mice), and PLX5622 chow replaced with control chow ($n = 6$ cochleae from 6 mice). Data are mean ± SD. ****$p < 0.0001$; ***$p < 0.001$; one-way ANOVA, Dunnett's multiple comparisons test. ns, not significant.

mean ABR threshold shifts at 16 kHz ($p = 0.19$), 22.6 kHz ($p = 0.40$), and 32 kHz ($p = 0.99$) between 1 and 15 DPNE (two-way ANOVA, Sidak's multiple comparison test). Similar to the results detected with PTS-inducing exposure, mice that were initially treated with PLX5622 and then replaced and maintained on control chow immediately after noise exposure (to allow macrophage repopulation) also significantly recovered the ABR thresholds after a TTS exposure (Fig. 8*A*, right). In addition, there was a significant reduction in DPOAE levels at 1 d after TTS noise exposure compared with the baseline levels. The reduced DPOAE levels recovered by 15 DPNE similar to baseline levels ($p < 0.0001$ baseline vs 1 DPNE [in all three groups]; $p = 0.11$ [control chow], $p = 0.44$ [PLX5622 chow], $p = 0.18$ [PLX5622 to control chow], 15 DPNE vs baseline, two-way ANOVA, Tukey's multiple comparison test) (Fig. 8*B*).

We also analyzed ABR Peak 1 amplitude and latency at 16 and 22.6 kHz at baseline, 1 and 15 DPNE to a mild TTS-imparting noise level of 90 dB SPL. Similar to the data above, at 16 kHz, the reduced ABR Peak 1 amplitude detected at 1 d after exposure was almost completely restored to baseline amplitude in the presence of both cochlear resident and repopulated macrophages (Fig. 9*A*,*E*). The recovered suprathreshold amplitude at 15 d recovery in control and PLX5622 to control treatment groups was comparable with the amplitude at prenoise exposure ($p = 0.46$ and $p = 0.93$, one-way ANOVA, Tukey's multiple comparison test) (Fig. 9*A*,*E*). Unlike with PTS exposure of 93 dB SPL shown above, both cochlear resident and repopulated macrophages partially yet significantly restored the reduced ABR Peak 1 amplitude to baseline amplitude at 22.6 kHz (Fig. 9*C*,*G*). Notably, such recovery was not found in mice that were maintained on PLX5622 treatment for the entire experiment at either 16 or 22.6 kHz (Fig. 9*A*,*C*,*E*,*G*). ABR Peak 1 latencies at 16 and 22.6 kHz were not significantly altered in the three experimental groups at any recovery period after exposure at 90 dB SPL (Fig. 9*B*,*D*,*F*,*H*). Together, these functional data corroborate with the data from PTS-inducing exposure and indicate that resident cochlear macrophages perform a critical function in recovering from mild TTS exposure independent of OHC functional recovery, and influence the restoration of ABR Peak 1 amplitudes as a function of synaptic repair.

Macrophages promote synaptic repair after TTS exposure

Last, to determine whether functional recovery of ABR Peak 1 amplitudes positively correlates with structural synaptic recovery, we performed synaptic immunolabeling on cochleae from mice fed on control chow, PLX5622-containing chow, and PLX5622-fed mice that were returned to control chow at 4 weeks after a TTS-imparting noise trauma for 2 h at 90 dB SPL (8-16 kHz). Data analysis revealed a significant recovery of IHC ribbon synapses in the middle region of the cochlea (16-22 kHz, same region where ABR P1 amplitude is measured) in mice fed on control chow and in PLX5622-fed mice that were returned to control chow (Fig. 10*A*,*B*). After 4 weeks recovery, the cochleae of exposed control mice and of PLX5622-fed mice that were returned to control chow possessed on average 17 ± 1.6 and 16 ± 1.4 synapses per IHC, respectively, which were statistically insignificant between the two groups ($p = 0.16$, one-way ANOVA). In contrast, mice that were fed PLX5622-containing chow for the entire duration of the experiment showed no evidence for synaptic repair, and the cochleae of these mice possessed 10 ± 1.3 synapses per IHC, which is significantly different from the exposed control mice and PLX5622-fed mice that were returned to control chow ($p \leq 0.0001$, one-way ANOVA) (Fig. 10*B*). These data show that macrophages also restore synapses following a mild TTS noise exposure.

Discussion

Our findings provide the first direct evidence for synaptic repair in the presence of cochlear macrophages and suggest that macrophages serve as key mediators of recovery of hearing, structural and functional repair of damaged IHC ribbon synapses, and neuron survival following noise-induced cochlear synaptopathy. Our data also indicate that initial loss of hearing and ribbon synapses because of noise exposure is independent of the presence or absence of macrophages (Fig. 11).

Macrophage depletion and repopulation in the cochlea

Cochlear macrophages can be eliminated using irradiation (Sato et al., 2008) or genetic methods, such as CD11b-DTR, CX_3CR1-DTR, or Csf1r-null mice (Brown et al., 2017; Hirose and Li, 2019; Kishimoto et al., 2019). We used a pharmacological method of oral delivery of inhibitor of CSF1R tyrosine kinase activity, PLX5622 in healthy adult mice and achieved a nearly complete (~94%) elimination of resident macrophages in the entire cochlea after 10 d of continuous PLX5622 chow treatment. In the CNS, it takes at least 3 d for microglia to die >90% after sustained exposure to CSF1R inhibitors (Elmore et al., 2014). The magnitude of macrophage depletion is found to be comparable between the genetic and pharmacological methods, with the latter being more efficient because of oral administration, penetration through the blood–brain barrier, presumably blood labyrinth barrier, and avoiding the need of repeated systemic injections of toxins in transgenic mice (Brown et al., 2017; Hirose and Li, 2019). Additionally, treatment with CSF1R inhibitor avoided the occurrence of the

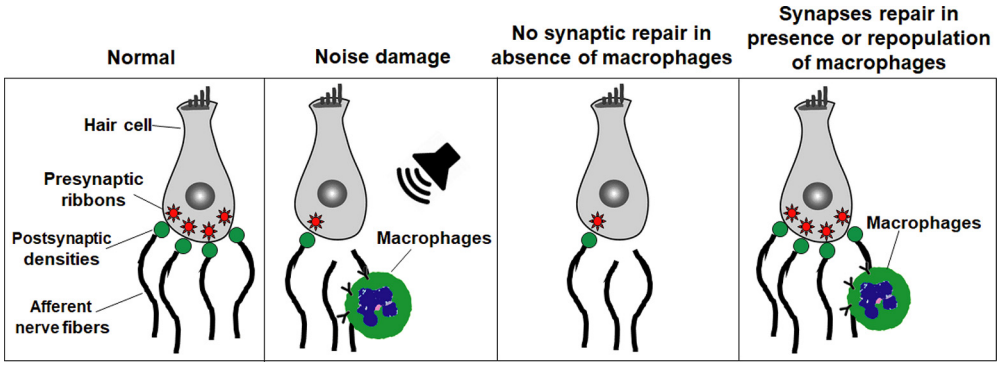

Figure 11. Scheme of macrophages promote repair of damaged IHC ribbon synapses after noise-induced cochlear synaptopathy. Compared with normal cochlea, prolonged or loud exposure to noise results in rapid loss of IHC ribbon synapses, retraction of afferent nerve fibers, and migration of resident macrophages into the damaged IHC synaptic region. In the absence of macrophages, the noise-damaged IHC ribbon synapses do not undergo spontaneous repair; however, the presence of resident macrophages or repopulated macrophages promotes structural and functional repair of noise-damaged IHC ribbon synapses.

undesired cytokine storm that can be observed in genetic models (Bruttger et al., 2015). In order to harness the reported beneficial effects of macrophages in the future, it will be helpful to study the rate and degree of elimination of cochlear macrophages following different doses of PLX5622.

There are two subtypes of resident macrophages present in the embryonic cochlea: Csf1r-dependent macrophages that originate from the yolk sac and Csf1r-independent CD11b-positive macrophages that appear to be derived from the fetal liver via systemic circulation. Indeed, in *Csf1r-null* mice, the density of Csf1r-dependent macrophages is significantly reduced without affecting the density of Csf1r-independent CD11b-positive macrophages (Kishimoto et al., 2019). Although it remains undetermined whether the two subtypes of resident macrophages persist in adulthood, there is a high likelihood that the remaining ~6% of resident macrophages that are unaffected by the PLX5622 treatment could be the Csf1r-independent CD11b-positive macrophages. Several studies have claimed that PLX5622 is microglia-specific and has no to little effects on the peripheral immune cells expressing CSF1R (Chitu et al., 2012; Elmore et al., 2014; Mok et al., 2014; Valdearcos et al., 2014; Spangenberg et al., 2016; Szalay et al., 2016). On the contrary, few studies have reported that PLX5622 does reduce the population of resident macrophages of peripheral tissues (Han et al., 2020; Lei et al., 2020). In our data using flow cytometry, PLX5622 treatment did not significantly impact the densities of different leukocytes in the peripheral tissues, similar to data reported in other published studies (Szalay et al., 2016; Lei et al., 2020). These discrepancies can be attributed to the dose and duration of PLX5622, or use of other CSF1R inhibitors, age of animals, or to the injury model.

Removal of PLX5622 causes rapid macrophage replenishment into the cochlea, and numbers of macrophages reach baseline levels within a week and are maintained up to 45 d of examination in the present study. A key question is as follows: what is the origin of these repopulated macrophages? CNS studies have demonstrated nestin-expressing microglial progenitors, and blood as the origin for repopulated microglia after selective elimination of microglia (>99%) in adult mice (Varvel et al., 2012; Elmore et al., 2014). However, a recent study using fate mapping and parabiosis provided convincing evidence that repopulated microglia are solely derived from the proliferation of residual microglia unaffected by PLX5622 after acute depletion (Huang et al., 2018). Our data demonstrate that repopulated macrophages promote recovery of hearing function, synaptic repair, and neuronal survival in a manner similar to the original cochlear resident macrophages. These data suggest that repopulated macrophages may inherit the phenotype of original resident macrophages. Further characterization of the newly repopulated macrophages in terms of their origin, distribution, morphology, activation, inflammatory profile, and function in healthy and damaged adult cochlea is required.

Macrophages and IHC ribbon synaptic repair

Both cochlear original resident and repopulated macrophages promote structural and functional repair of noise-damaged IHC ribbon synapses to a similar degree, suggesting that macrophages directly impact the IHC synapses. The synaptic repair detected with repopulated macrophages could be partly attributed to the effect of PLX5622 removal; however, we did not test this hypothesis directly in the present study. To address this, future studies are needed wherein a second macrophage depletion model (e.g., CX_3CR1-DTR mouse model) (Buch et al., 2005; Hirose and Li, 2019) is combined with PLX5622 removal to prevent repopulation of macrophages to determine whether it is repopulated macrophages but PLX5622 removal specifically that promotes synaptic repair. Furthermore, use of CX_3CR1-DTR mouse as an additional genetic tool to eliminate cochlear macrophages will verify our present conclusions with PLX5622 as a pharmacological tool.

It is unclear how macrophages facilitate restoration of cochlear synapses and function and remain an important future perspective. We have previously shown that the intact endogenous fractalkine signaling axis (CX_3CL1-CX_3CR1), whereby CX_3CL1 (ligand) is a chemokine that is constitutively expressed by IHCs and SGNs and CX_3CR1 receptors are exclusively present on cochlear macrophages, plays a key role in repair of the noise-damaged ribbon synapses (Kaur et al., 2019). CNS studies have also shown that microglia are active players in controlling development and remodeling of excitatory synapses and neural circuit formation by phagocytic engulfment and elimination of synapses partly via fractalkine signaling axis (Tremblay et al., 2010; Paolicelli et al., 2011, 2014; Schafer et al., 2012; Weinhard et al., 2018; Marinelli et al., 2019; Basilico et al., 2022). In the future, it will be important to examine whether CX_3CL1/CX_3CR1 axis influences PLX5622-induced lack of synaptic repair or PLX5622 to control-induced synaptic repair to determine the exact role of CX_3CL1/CX_3CR1 axis in macrophage-mediated synaptic repair.

Macrophages and recovery of auditory functional defects

PLX5622-mediated elimination of resident macrophages in uninjured mature cochlea did not adversely affect ABR thresholds,

ABR Peak 1 amplitudes, and latencies and DPOAEs. Our data support the findings reported by Hirose and Li (2019), which showed that targeted depletion of CX_3CR1-expressing macrophages in adult *CX_3CR1-DTR* mice did not alter the baseline ABR thresholds (Hirose and Li, 2019). The most intriguing and unexpected finding in the present study is the complete to partial recovery of ABR thresholds and ABR Peak 1 amplitudes after TTS- or PTS-inducing noise trauma, respectively, in mice with cochlear resident and repopulated macrophages. With PTS-inducing noise trauma, although there is near to complete restoration of IHC synapses in the middle region of the cochlea, the recovery of diminished ABR Peak 1 amplitudes at similar cochlear frequencies is incomplete. These data may imply that there is damage to other structures or parts of IHCs and SGNs beyond the synapses that do not undergo repair. The exact reasons for these observations are unclear and need to be carefully resolved in the future.

Unlike in the normal mature cochlea, transient depletion of cochlear macrophages during early auditory nerve development results in auditory functional impairment that partially recovers in adulthood (Brown et al., 2017). Similarly, temporary postnatal microglia depletion in the brainstem significantly elevates auditory thresholds that are restored to normal thresholds by 7 weeks after microglia repopulation (Milinkeviciute et al., 2021). Notably, PLX5622 treatment depletes both cochlear macrophages and brain microglia, and it remains uncertain whether PLX5622 treatment and microglial depletion effect the central auditory nuclei. Systematic investigation of microglia density, neuronal survival, and synapse numbers in the central auditory pathway and correlation with later ABR peaks (II-V) with PLX5622 treatment and after synaptopathic noise exposure are required. Furthermore, restricted elimination of either microglia or cochlear macrophages may help address these issues and determine whether cochlear macrophages and microglia have unique or similar effects on different aspects of ABRs in noise-induced hearing loss. Currently, we cannot selectively eliminate cochlear macrophages or brain microglia to evaluate the individual roles of these cells on different aspects of ABRs after noise-induced cochlear injury.

Currently, we do not understand the mechanisms by which cochlear resident and repopulated macrophages influence the recovery of ABR thresholds after noise trauma, but the data imply that macrophages may directly impact the functional properties of IHCs, synapses, and/or Type I SGNs that contribute to generation of ABRs without significantly impacting the function of OHCs. Previously, we did not observe restoration or exacerbation of cochlear function after profound sensorineural hearing loss where sensory hair cells and neurons are damaged and/or lost (Kaur et al., 2015, 2018). These data imply that macrophages may perform functional protective role in a context-dependent manner that is related to the degree of tissue damage and hearing loss.

In conclusion, every form of sensorineural hearing loss is associated with an increased macrophage immune response in the cochlea, yet the functions of these innate immune cells remain unclear. Our work has revealed a novel endogenous cellular mechanism for cochlear resident macrophages in promoting IHC ribbon synaptic repair, SGN survival and influencing recovery of loss of cochlear function following an acute synaptopathic noise exposure. Further understanding of mechanisms by which macrophages promote synaptic repair and determining properties of such repaired synapses will urge the development of putative immunotherapies to preserve neurons and regenerate synapses to treat noise- or age-related hidden hearing loss and associated perceptual anomalies. Finally, our findings can be extended to chronic forms of sensorineural hearing loss whereby dysfunctional or chronically activated macrophages can be eliminated and repopulated with functional macrophages as a potential approach to mitigate ototoxic drugs-, noise-, infection-, or age-related hearing loss that is associated with chronic inflammation likely because of dysfunctional macrophages.

References

Basilico B, Ferrucci L, Ratano P, Golia MT, Grimaldi A, Rosito M, Ragozzino D (2022) Microglia control glutamatergic synapses in the adult mouse hippocampus. Glia 70:173–195.

Bramhall NF, Konrad-Martin D, McMillan GP, Griest SE (2017) Auditory brainstem response altered in humans with noise exposure despite normal outer hair cell function. Ear Hear 38:e1–e12.

Bramhall NF, Konrad-Martin D, McMillan GP (2018) Tinnitus and auditory perception after a history of noise exposure: relationship to auditory brainstem response measures. Ear Hear 39:881–894.

Bramhall NF, McMillan GP, Gallun FJ, Konrad-Martin D (2019) Auditory brainstem response demonstrates that reduced peripheral auditory input is associated with self-report of tinnitus. J Acoust Soc Am 146:3849.

Bramhall NF, Niemczak CE, Kampel SD, Billings CJ, McMillan GP (2020) Evoked potentials reveal noise exposure-related central auditory changes despite normal audiograms. Am J Audiol 29:152–164.

Brown LN, Xing Y, Noble KV, Barth JL, Panganiban CH, Smythe NM, Lang H (2017) Macrophage-mediated glial cell elimination in the postnatal mouse cochlea. Front Mol Neurosci 10:407.

Bruttger J, Karram K, Wörtge S, Regen T, Marini F, Hoppmann N, Klein M, Blank T, Yona S, Wolf Y, Mack M, Pinteaux E, Müller W, Zipp F, Binder H, Bopp T, Prinz M, Jung S, Waisman A (2015) Genetic cell ablation reveals clusters of local self-renewing microglia in the mammalian central nervous system. Immunity 43:92–106.

Buch T, Heppner FL, Tertilt C, Heinen TJ, Kremer M, Wunderlich FT, Jung S, Waisman A (2005) A Cre-inducible diphtheria toxin receptor mediates cell lineage ablation after toxin administration. Nat Methods 2:419–426.

Chitu V, Nacu V, Charles JF, Henne WM, McMahon HT, Nandi S, Ketchum H, Harris R, Nakamura MC, Stanley ER (2012) PSTPIP2 deficiency in mice causes osteopenia and increased differentiation of multipotent myeloid precursors into osteoclasts. Blood 120:3126–3135.

Dagher NN, Najafi AR, Kayala KM, Elmore MR, White TE, Medeiros R, West BL, Green KN (2015) Colony-stimulating factor 1 receptor inhibition prevents microglial plaque association and improves cognition in 3xTg-AD mice. J Neuroinflammation 12:139.

Elmore MR, Najafi AR, Koike MA, Dagher NN, Spangenberg EE, Rice RA, Kitazawa M, Matusow B, Nguyen H, West BL, Green KN (2014) Colony-stimulating factor 1 receptor signaling is necessary for microglia viability, unmasking a microglia progenitor cell in the adult brain. Neuron 82:380–397.

Elmore MR, Lee RJ, West BL, Green KN (2015) Characterizing newly repopulated microglia in the adult mouse: impacts on animal behavior, cell morphology, and neuroinflammation. PLoS One 10:e0122912.

Fernandez KA, Guo D, Micucci S, De Gruttola V, Liberman MC, Kujawa SG (2020) Noise-induced cochlear synaptopathy with and without sensory cell loss. Neuroscience 427:43–57.

Furman AC, Kujawa SG, Liberman MC (2013) Noise-induced cochlear neuropathy is selective for fibers with low spontaneous rates. J Neurophysiol 110:577–586.

GBD 2019 Hearing Loss Collaborators (2021) Hearing loss prevalence and years lived with disability, 1990-2019: findings from the Global Burden of Disease Study 2019. Lancet 397:996–1009.

Han J, Fan Y, Zhou K, Zhu K, Blomgren K, Lund H, Harris RA (2020) Underestimated peripheral effects following pharmacological and conditional genetic microglial depletion. Int J Mol Sci 21:8603.

Hickman TT, Hashimoto K, Liberman LD, Liberman MC (2020) Synaptic migration and reorganization after noise exposure suggests regeneration in a mature mammalian cochlea. Sci Rep 10:19945.

Hickman TT, Hashimoto K, Liberman LD, Liberman MC (2021) Cochlear synaptic degeneration and regeneration after noise: effects of age and neuronal subgroup. Front Cell Neurosci 15:684706.

Hickox AE, Liberman MC (2014) Is noise-induced cochlear neuropathy key to the generation of hyperacusis or tinnitus? J Neurophysiol 111:552–564.

Hirose K, Li SZ (2019) The role of monocytes and macrophages in the dynamic permeability of the blood-perilymph barrier. Hear Res 374:49–57.
Huang Y, Xu Z, Xiong S, Sun F, Qin G, Hu G, Peng B (2018) Repopulated microglia are solely derived from the proliferation of residual microglia after acute depletion. Nat Neurosci 21:530–540.
Kaur T, Zamani D, Tong L, Rubel EW, Ohlemiller KK, Hirose K, Warchol ME (2015) Fractalkine signaling regulates macrophage recruitment into the cochlea and promotes the survival of spiral ganglion neurons after selective hair cell lesion. J Neurosci 35:15050–15061.
Kaur T, Ohlemiller KK, Warchol ME (2018) Genetic disruption of fractalkine signaling leads to enhanced loss of cochlear afferents following ototoxic or acoustic injury. J Comp Neurol 526:824–835.
Kaur T, Clayman AC, Nash AJ, Schrader AD, Warchol ME, Ohlemiller KK (2019) Lack of fractalkine receptor on macrophages impairs spontaneous recovery of ribbon synapses after moderate noise trauma in C57BL/6 mice. Front Neurosci 13:620.
Kim KX, Payne S, Yang-Hood A, Li SZ, Davis B, Carlquist J, Rutherford MA (2019) Vesicular glutamatergic transmission in noise-induced loss and repair of cochlear ribbon synapses. J Neurosci 39:4434–4447.
Kishimoto I, Okano T, Nishimura K, Motohashi T, Omori K (2019) Early development of resident macrophages in the mouse cochlea depends on yolk sac hematopoiesis. Front Neurol 10:1115.
Kujawa SG, Liberman MC (2009) Adding insult to injury: cochlear nerve degeneration after 'temporary' noise-induced hearing loss. J Neurosci 29:14077–14085.
Le TN, Straatman LV, Lea J, Westerberg B (2017) Current insights in noise-induced hearing loss: a literature review of the underlying mechanism, pathophysiology, asymmetry, and management options. J Otolaryngol Head Neck Surg 46:41.
Lei F, Cui N, Zhou C, Chodosh J, Vavvas DG, Paschalis EI (2020) CSF1R inhibition by a small-molecule inhibitor is not microglia specific: affecting hematopoiesis and the function of macrophages. Proc Natl Acad Sci USA 117:23336–23338.
Liberman LD, Suzuki J, Liberman MC (2015) Dynamics of cochlear synaptopathy after acoustic overexposure. J Assoc Res Otolaryngol 16:205–219.
Lin HW, Furman AC, Kujawa SG, Liberman MC (2011) Primary neural degeneration in the Guinea pig cochlea after reversible noise-induced threshold shift. J Assoc Res Otolaryngol 12:605–616.
Marinelli S, Basilico B, Marrone MC, Ragozzino D (2019) Microglia-neuron crosstalk: signaling mechanism and control of synaptic transmission. Semin Cell Dev Biol 94:138–151.
Milinkeviciute G, Chokr SM, Cramer KS (2021) Auditory brainstem deficits from early treatment with a CSF1R inhibitor largely recover with microglial repopulation. eNeuro 8:ENEURO.0318-20.2021.
Mok S, Koya RC, Tsui C, Xu J, Robert L, Wu L, Graeber T, West BL, Bollag G, Ribas A (2014) Inhibition of CSF-1 receptor improves the antitumor efficacy of adoptive cell transfer immunotherapy. Cancer Res 74:153–161.
Paolicelli RC, Bolasco G, Pagani F, Maggi L, Scianni M, Panzanelli P, Giustetto M, Ferreira TA, Guiducci E, Dumas L, Ragozzino D, Gross CT (2011) Synaptic pruning by microglia is necessary for normal brain development. Science 333:1456–1458.
Paolicelli RC, Bisht K, Tremblay ME (2014) Fractalkine regulation of microglial physiology and consequences on the brain and behavior. Front Cell Neurosci 8:129.
Rojo R, et al. (2019) Deletion of a Csf1r enhancer selectively impacts CSF1R expression and development of tissue macrophage populations. Nat Commun 10:3215.
Sato E, Shick HE, Ransohoff RM, Hirose K (2008) Repopulation of cochlear macrophages in murine hematopoietic progenitor cell chimeras: the role of CX3CR1. J Comp Neurol 506:930–942.
Schafer DP, Lehrman EK, Kautzman AG, Koyama R, Mardinly AR, Yamasaki R, Ransohoff RM, Greenberg ME, Barres BA, Stevens B (2012) Microglia sculpt postnatal neural circuits in an activity and complement-dependent manner. Neuron 74:691–705.
Sergeyenko Y, Lall K, Liberman MC, Kujawa SG (2013) Age-related cochlear synaptopathy: an early-onset contributor to auditory functional decline. J Neurosci 33:13686–13694.
Shi L, Liu K, Wang H, Zhang Y, Hong Z, Wang M, Wang X, Jiang X, Yang S (2015) Noise induced reversible changes of cochlear ribbon synapses contribute to temporary hearing loss in mice. Acta Otolaryngol 135:1093–1102.
Shi L, Liu L, He T, Guo X, Yu Z, Yin S, Wang J (2013) Ribbon synapse plasticity in the cochleae of Guinea pigs after noise-induced silent damage. PLoS One 8:e81566.
Sliwinska-Kowalska M, Zaborowski K (2017) WHO environmental noise guidelines for the European region: a systematic review on environmental noise and permanent hearing loss and tinnitus. Int J Environ Res Public Health 14:1139.
Song Q, Shen P, Li X, Shi L, Liu L, Wang J, Yu Z, Stephen K, Aiken S, Yin S, Wang J (2016) Coding deficits in hidden hearing loss induced by noise: the nature and impacts. Sci Rep 6:25200.
Spangenberg EE, Lee RJ, Najafi AR, Rice RA, Elmore MR, Blurton-Jones M, West BL, Green KN (2016) Eliminating microglia in Alzheimer's mice prevents neuronal loss without modulating amyloid-beta pathology. Brain 139:1265–1281.
Stanley ER, Berg KL, Einstein DB, Lee PS, Pixley FJ, Wang Y, Yeung YG (1997) Biology and action of colony–stimulating factor-1. Mol Reprod Dev 46:4–10.
Suthakar K, Liberman MC (2021) Auditory-nerve responses in mice with noise-induced cochlear synaptopathy. J Neurophysiol 126:2027–2038.
Szalay G, Martinecz B, Lénárt N, Környei Z, Orsolits B, Judák L, Császár E, Fekete R, West BL, Katona G, Rózsa B, Dénes Á (2016) Microglia protect against brain injury and their selective elimination dysregulates neuronal network activity after stroke. Nat Commun 7:11499.
Tremblay ME, Lowery RL, Majewska AK (2010) Microglial interactions with synapses are modulated by visual experience. PLoS Biol 8:e1000527.
Valdearcos M, Robblee MM, Benjamin DI, Nomura DK, Xu AW, Koliwad SK (2014) Microglia dictate the impact of saturated fat consumption on hypothalamic inflammation and neuronal function. Cell Rep 9:2124–2138.
Valero MD, Burton JA, Hauser SN, Hackett TA, Ramachandran R, Liberman MC (2017) Noise-induced cochlear synaptopathy in rhesus monkeys (*Macaca mulatta*). Hear Res 353:213–223.
Varvel NH, Grathwohl SA, Baumann F, Liebig C, Bosch A, Brawek B, Thal DR, Charo IF, Heppner FL, Aguzzi A, Garaschuk O, Ransohoff RM, Jucker M (2012) Microglial repopulation model reveals a robust homeostatic process for replacing CNS myeloid cells. Proc Natl Acad Sci USA 109:18150–18155.
Viana LM, O'Malley JT, Burgess BJ, Jones DD, Oliveira CA, Santos F, Merchant SN, Liberman LD, Liberman MC (2015) Cochlear neuropathy in human presbycusis: confocal analysis of hidden hearing loss in post-mortem tissue. Hear Res 327:78–88.
Weinhard L, di Bartolomei G, Bolasco G, Machado P, Schieber NL, Neniskyte U, Exiga M, Vadisiute A, Raggioli A, Schertel A, Schwab Y, Gross CT (2018) Microglia remodel synapses by presynaptic trogocytosis and spine head filopodia induction. Nat Commun 9:1228.
World Health Organization (2021) World report on hearing. Available at https://www.who.int/publications/i/item/world-report-on-hearing.
Wu PZ, O'Malley JT, de Gruttola V, Liberman MC (2021) Primary neural degeneration in noise-exposed human cochleas: correlations with outer hair cell loss and word-discrimination scores. J Neurosci 41:4439–4447.